In-Band Pumped Conical Refraction Lasers Based on the Nd:$KGd(WO_4)_2$ Crystal

By
Chandan Qumar Howlader

A Thesis submitted to the Faculty of Graduate Studies of
The University of Manitoba
In partial fulfillment of the requirements of the degree of

MASTER OF SCIENCE

Department of Electrical and Computer Engineering
University of Manitoba
Winnipeg

Abstract

The laser has been used in many areas of science and technology. At the same time there are different types of lasers and conical refraction (CR) laser is one of them. Recently, there has been a strong interest in conical refraction lasers and their applications. CR lasers have the potential applications in areas like optical trapping, free space communication, super-resolution microscopy, quantum computing, cryptography, polarization demultiplexing and multiplexing, polarimetry, mode conversion and so on.

The biaxial crystal of Neodymium-doped potassium gadolinium tungstate (Nd:KGW) has been used to produce a CR laser output with in-band pumping. Unfortunately, the thermal conductivity of this crystal is relatively low which limits the high-power operation even for in-band pumping at longer wavelength which decreases the quantum defect and leads to a significant reduction of thermal load in the crystal. This thesis addressed this aspect by proposing a "passive" CR laser scheme.

In this work, we demonstrated two types of CR lasers, an active CR laser and a passive CR laser. In active CR laser the functions of laser gain medium and CR element are performed by the same crystal. In passive CR laser these functions are separated: the laser radiation is produced by one crystal and CR is done by the other. The active CR Nd:KGW laser produced and output power of 1.15 W with 32% of slope efficiency and 25.6% optical to optical efficiency. The characteristic hollow ring of the CR laser mode was not observed because the incident laser beam diameter was very large compared to the CR ring diameter supported by the crystal. For passive CR laser, Nd:KGW crystal was placed inside the Nd:YVO laser cavity and a CR ring has been seen with the proper alignment. The CR operation was confirmed by comparing the laser beam shape with a reference He-Ne laser beam passed through the Nd:KGW crystal in a separate experiment. For 10.8 W of absorbed pump power the maximum obtained CR laser output power was 3.68 W, thus demonstrating feasibility of dual crystal CR laser and its power scalability.

Acknowledgements

I am very thankful to my supervisor Dr. Arkady Major for giving me an opportunity to work in his laser photonics research group. This research could not have been accomplished without his proper guidance. Throughout my master's program I have learned a lot from him. He was generous to provide solution not only in academic purpose but also in daily life. I am also grateful to our collaborators Prof. Edik Rafailov and Dr. Ksenia Fedorova from Aston University, UK, and Prof. Grigorii Sokolovskii, Ioffe Institute, Russia, who provided the CR laser crystal and valuable suggestions to gear up my research.

Throughout the course of experiment my group members Tanant Waritanant, Mohammad Nadimi as well as Reza Akbari guided me to start experimental work and helped me to understand the practical work. In addition, Rubel Chandra Talukder extended his helping hand for the clarification of any kind of ambiguity. I also would like to thank my other groupmates Sujith, Shirin, Anisur for sharing their knowledge which gave fuel to my work.

I would also like to thank the Manitoba provincial government, University of Manitoba graduate student associations' (UMGSA), the University of Manitoba as well as Natural Sciences and Engineering Research Council (NSERC) for financial support.

Finally, I would like to thank my father and sisters for accepting my interest to study overseas. Special thanks to my beloved wife for standing beside me for my desire.

Table of Contents

List of Figures

List of Tables

Chapter 1: Introduction

1.1 Motivation:

Schawlow and Townes were first to formulate the condition for laser action at the optical frequency in 1958 and Maiman demonstrated this experimentally in 1960 using a crystalline solid system. Within five decades, the laser has been used in many fields of commercial and fundamental areas of science there are such continuous wave laser, pulsed laser, ultra-fast laser. Among different types of lasers there is a special type of laser known as a conical refraction (CR) laser and this type of lasers is attractive for applications like optical trapping, free space communication, super-resolution microscopy, quantum computing, cryptography, polarization demultiplexing and multiplexing, polarimetry, mode conversion and so on [1-3]. The special CR beam pattern and state of polarization are important for these applications. When compared to a Gaussian beam, CR beam has a ring-shaped pattern with null intensity at the center in the near field but in the far field it evolves back to the Gaussian beam.

To obtain CR laser, a laser medium should be biaxial. Fortunately, the well-known laser crystal of Nd:KGW is biaxial in nature as well as a popular laser gain medium. For instance, it has higher doping concentration as compared with most commonly used laser media like Nd:YAG and Nd:YVO. Its anisotropic properties lead to polarized laser radiation which is advantageous for nonlinear effect such as second-harmonic generation [4]. In contrast with Nd:YAG, it has a lower upper state life time, higher emission cross section which is good for efficient continuous wave laser operation [5]. Furthermore, it is a very good medium for Raman frequency conversion [4]. Also, the biaxial nature results in double refraction which is one of the primary condition for conical refraction (CR) [6]. For CR one of the defining parameters is semi-angle which is larger in Nd:KGW as compared to Aragonite and $KTiOPO_4$ [7]. Aragonite was used to observe the CR in the very beginning by Lloyd [8].

In spite of this, Nd:KGW has an inferior thermal properties which lead to higher thermal gradients in the crystal and hinders high power operation. This thermal gradient results in refractive index change through the thermo-optic effect, mechanical stress, and surface bulging [9]. As a result, thermal lensing is introduced which reduces the laser output beam quality and

optical efficiency and at last, the laser crystal can be damaged. To overcome this effect we need to reduce the main heat source named as the quantum defect. This can be done by pumping at a wavelength closer to the laser wavelength, which is usually called in-band pumping. Pumping at 910 nm for Nd:KGW reduces the quantum defect by more than 46% as compared to conventional 808 nm pumping method [10]. Power scaling is still challenging due to relatively low thermal conductivity of Nd:KGW crystal. However, there is another way to get CR laser: a laser radiation generated elsewhere can pass through a conical refraction medium. This type of set up could be suitable for power scaling. For example, Nd:YVO is a good choice for such case because of its higher thermal conductivity and higher emission cross section than of Nd:KGW [9]. Therefore, using Nd:YVO as a laser medium and Nd:KGW as an intracavity CR element would be a good strategy to obtain higher output power. At the same time it was also reported that in-band pumping of Nd:YVO at 914 nm reduces the thermal lensing strength to the level of half as compared to traditional 808nm pumping [9]. In addition, another in-band pumping study for Nd:YVO reported the slope efficiency up to 80.7 % in CW regime [11] and up to 77.1% in the mode-locked regimes [12]. Additionally, Yb:KGW CR laser has been pumped at 980 nm and obtained 8.6 W with 60.5% slope efficiency which is the same as the standard Yb:KGW laser [13].

For this reason, a pumping scheme of 910 nm has been used to pump both the Nd:KGW and Nd:YVO laser crystals to get active and passive CR, respectively, in the continuous wave regime.

1.2 Objectives

The goal of this work was to demonstrate active CR and passive CR using the conical refraction phenomena for the laser gain medium Nd:KGW. Whereas Nd:KGW is the laser-active CR medium, Nd:YVO can only act as a laser medium. Moreover, in-band pumping at 910 nm was used to reduce the quantum defect as well as thermal lensing. Therefore, the low quantum defect pumping demonstrated in this work can open a new path for power scaling of CR lasers.

1.3 Contribution

We demonstrated the first Nd:KGW CR laser with in-band pumping. We also for the first time introduced passive conical refraction laser using a cascade of active laser gain medium and conical medium inside the optical cavity. This enabled us to obtain the highest CR laser output power to the best of my knowledge. The results of active and passive CR laser have been presented at Photonics North 2017 conference as a poster presentation.

1.4 Outline of the thesis

This thesis is divided into four parts. Chapter 2 describes the background theory of conical refraction followed by the description of uniaxial and biaxial crystals. Formation of CR ring pattern and its evolution as it propagates in space is also discussed. After that the optical and mechanical properties of Nd:KGW and Nd:YVO_4 laser crystals are discussed and compared with other commonly used laser materials.

In chapter 3, we have described the design of laser cavity as well as the experimental setup of the built CR lasers. Dependence of the beam diameter and cavity stability parameter on the thermal lens of the crystal has been shown. We also described the pumping technique and the effect of pump wavelength on the laser system.

Chapter 4 mainly presents the outcomes of my experiments. We have compared our results with the other CR works to highlight our achievements.

In chapter 5 conclusions and future work have been discussed.

Chapter 2: Background theory

2.1 Conical refraction

Conical refraction is a phenomenon which takes place only in a biaxial crystal when it is cut perpendicular to one of its optical axes and a narrow beam of light is incident along such an axis. It was predicted by Hamilton in 1832 theoretically [14] using Fresnel's wave theory [7] and published by Royal Irish Academy. Later on, Lloyd proved the theoretical prediction through an experiment. At that time it was very difficult to get good quality crystals to do the CR experiments. Before the twenty first century it was the primary limitation. Nowadays, crystal technology has been improved a lot and suitable crystals for CR are available. Therefore, people started working on CR both ways, theoretically and experimentally. CR is attractive for its characteristic and symmetric pattern forming along its propagation direction with zero intensity in the center and having any two opposite points on the ring to be orthogonally polarized [15] as shown in figure 2.1. CR is one of the examples of wave nature of light.

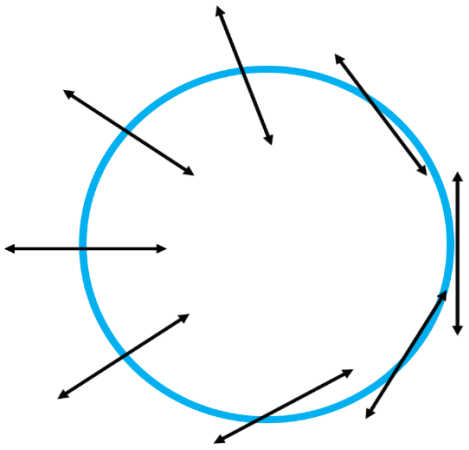

Figure 2.1: Schematic diagram of polarization along the ring of CR[2][16].

The propagation of light within a medium depends on the type of medium. If the medium properties (e.g. refractive index, conductivity) are independent of direction of propagation, then it is known as an isotropic medium. On the contrary, when properties of materials depend on the direction of propagation, it is known as an anisotropic medium. At the same time there are

two kinds of anisotropic media: uniaxial and biaxial. The refractive indices along two principal axes of the uniaxial crystal are equal and the refractive indices in a biaxial crystal are completely different along all three its principal axes. However, for uniaxial crystals Bartholin observed that two types of beams are refracted if light does not propagate along the optical axis [18]. One is called an ordinary beam and another one an extraordinary beam. Figures 2.2(a-c) show the transverse cuts of wave surfaces in XY, ZX and ZY planes respectively where X, Y and Z are three Cartesian coordinates. Wave (or phase) surface can be defined by the variation of refractive indices along the principal axes of the crystal. Depending on the polarization of incident wave it experiences different refractive indices along different directions. P-polarized or ordinary wave experiences the same refractive index independent of the direction and therefore makes a spheroid wave surface. But S-polarized or extraordinary wave experiences various refractive indices depending on the direction of propagation and thus makes an ellipsoid wave surface. These surfaces are also known as Fresnel wave surfaces. The line connecting the points at which the spheroid and ellipsoid touch each other (figure 2.2 (b,c)) is called an optical axis. Uniaxial crystals have only one such direction, i.e. only one optical axis. There are two types of uniaxial crystals: the case where spheroid is contained within the ellipsoid is known as a positive uniaxial crystal and the opposite one is called the negative uniaxial crystal.

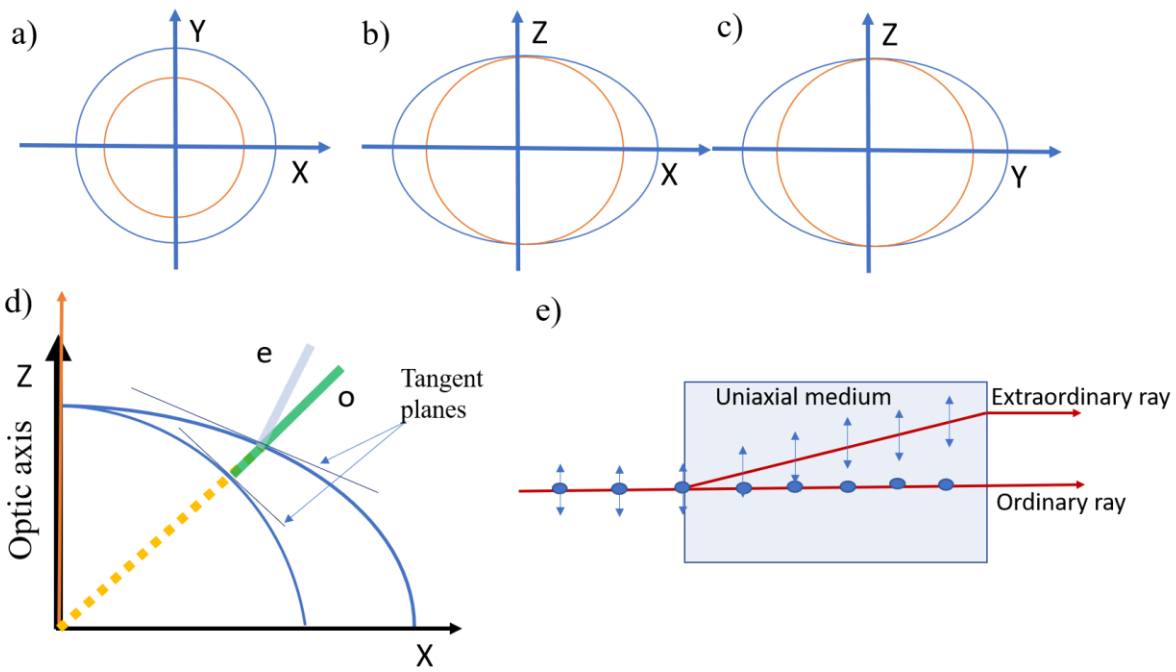

Figure 2.2: Schematic diagram of transverse cut of the wave surface of a uniaxial crystal in (a) XY plane, (a) ZX plane, (a) ZY plane, (d) an input plane wave refracted into an ordinary and extraordinary plane wave, (e) refraction of ray [17].

Figure 2.2 (d) illustrates the refraction of an input plane wave by a uniaxial crystal which happens in the direction of normal vectors (blue and green lines) to the tangent planes at the crossing point between the input ray and the Fresnel (phase) surfaces. This means that a beam propagating along the optical axis does not experience double refraction. Green line represents an ordinary beam which has a spherical wave front and follows the Snell's law and another one is an extraordinary beam which has an ellipsoid wave front. The direction of the extraordinary wave depends on the angle of incidence with optical axis. Furthermore, David Brewster discovered a few materials that don't have double refraction along two different directions which means that they have two optical axes. Such materials are known as biaxial crystals.

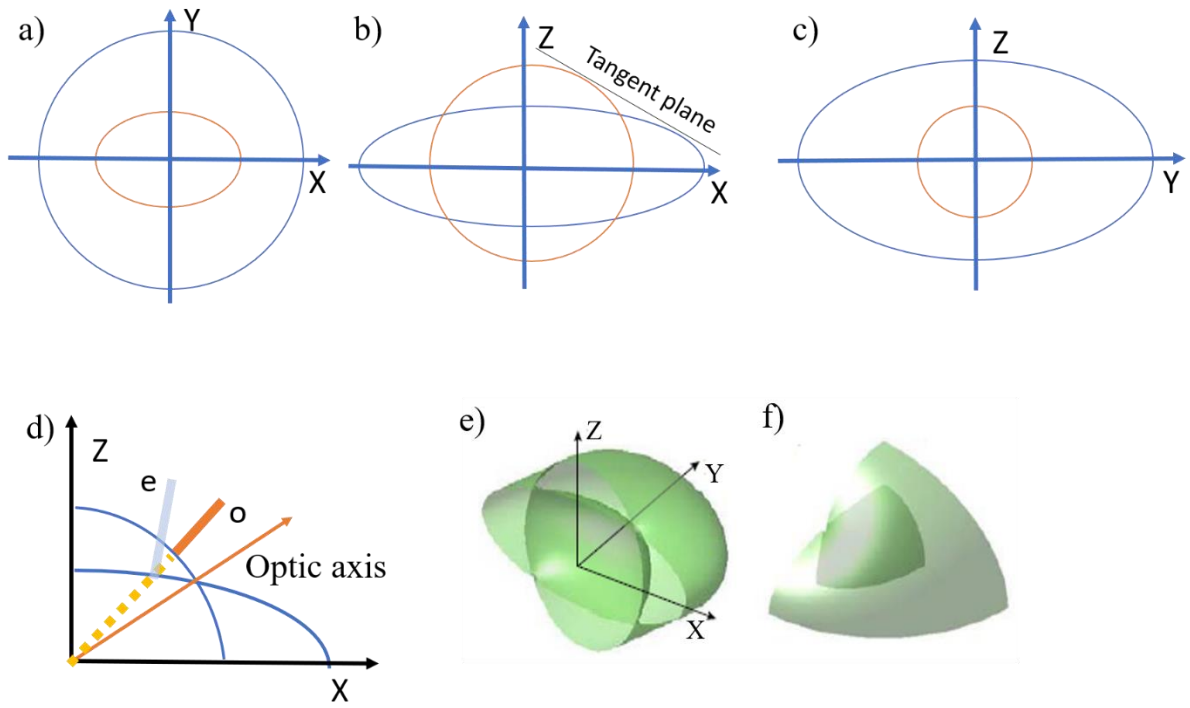

Figure 2.3: Schematic diagram of transverse cuts of the wave surface of a biaxial crystal in (a) XY plane, (a) ZX plane, (a) ZY plane, (d) an input plane wave refracted into an ordinary and extraordinary plane wave, (e) 3D representation of wave surface, (f) a single octane of wave surface to show the plane refraction along one of the optical axes [17].

Figure 2.3 shows the transverse cuts of wave surfaces in a biaxial crystal. As can be seen, in biaxial crystals propagation of the input plane wave is the same as in uniaxial crystals. It also should be noted that in this case the wave surfaces in biaxial crystals cross each other at 4 points showed in fig 2.3(b). If we connect the diametrically opposite two points we will get the directions of two optical axes. However, unlike in uniaxial crystals, a tangent plane cannot be defined at these crossing points, i.e. the light cannot propagate along the optical axes.

On the other hand, a tangent plane *enclosing* the optical axis can be defined which will touch two points of the wave surface as shown in figure 2.3 (b). In this situation light must follow the path inside the medium toward the intersection points of the tangent plane and wave surface (i.e. away from the optical axis). Quite importantly, in space the touching points of such a tangent plane and the wave surface will form a ring pattern.

Therefore, when a beam of light is incident along one of the optical axes of a biaxial crystal it should refract internally as a slanted cone within the crystal and emerge from it as a hollow

light cylinder whose transverse cross section forms a ring of light. If a focused beam of light is incident at the crystal and propagates as a pencil within the crystal it will emerge externally as a cone of light. These two new phenomena were called as internal and external conical refraction, respectively, by Hamilton and are shown in figure 2.4. Behavior of light such as the interference, diffraction and double refraction inside the uniaxial and biaxial crystals could be described by Fresnel's theory of light.

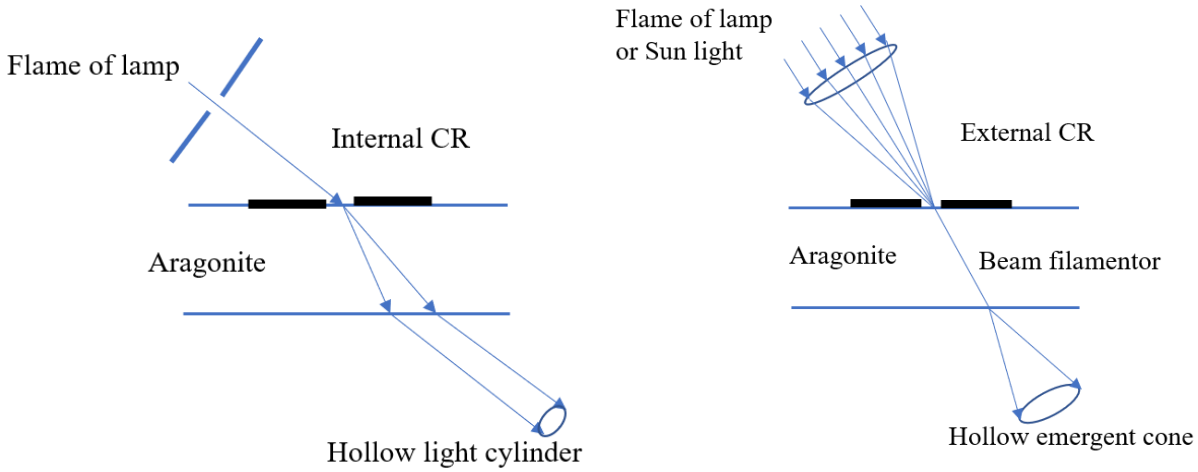

Figure 2.4: Schematic diagram of the experimental set up of Humphrey Lloyd to observe internal CR and external CR [8].

After theoretical prediction of CR by Hamilton, Lloyd experimentally observed these phenomena. At the same time he noticed that the opposite points along the ring experienced orthogonal polarizations shown in figure 2.1. To get a CR, the crystal must be cut perpendicular to one of the optical axes and it should have good optical quality [8]. The ring pattern depends on the polarization of the incident beam. For unpolarized and circularly polarized light the CR ring is a complete circle and for linearly polarized light the CR ring pattern has a crescent shape.

The angle of internal conical refraction cone depends on the refractive indices of the biaxial crystal. The relationship among the indices is $n_1<n_2<n_3$. There is another condition that $n_2 - n_1$ and $n_3 - n_2$ should be small compared with n_2, so that all refraction and diffraction effects are paraxial [6]. The schematic diagram of a focused beam of light propagating within the crystal as a hollow cone with a semi-angle A is shown in figure 2.5.

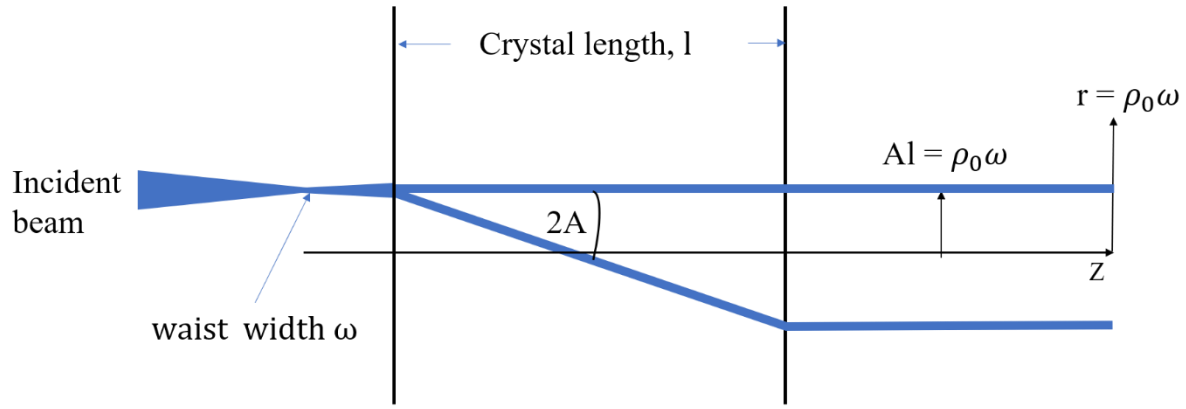

Figure 2.5: Schematic diagram forming cone inside the crystal [6]

Slanted hollow cylinder size can be calculated using the refractive indices and length of the crystal along the propagation direction. The semi-angle equation is given below by

$$A = \frac{1}{n2}\sqrt{(n2-n1)(n3-n2)},$$

where – n1, n2 and n3 are three refractive indices of a crystal.

The profile of beam that emerges after passing through the length *l* of the crystal depends on the following dimensionless variables

$$\rho_0 \equiv \frac{Al}{\omega}$$

$$\rho_0 \equiv \frac{r}{\omega},$$

where r is the ring radius and ω is the beam waist radius.

For our Nd:KGW laser crystal, we calculated the semi-angle as 17 mrad and the ring radius that could be produced was 306 µm. The condition to observe a CR ring clearly is ρ_0 >> 1; if ρ_0 is not large enough, the fine details are obscured by the beam width. The Belsky and Stepanov [17] found the relation between the ring radius r and the beam waist radius ω to clearly observe the ring pattern, i.e. r >> ω.

Furthermore, in 1839 Johann Christian Poggendorff observed that the light ring is not solid, it is split by a ring of complete darkness shown in figure 2.6. Later, Voigt gave explanation on the Poggendroff dark ring. The two rings are produced because of the ordinary and extraordinary polarizations and it is named as ordinary and extraordinary conical wave [17].

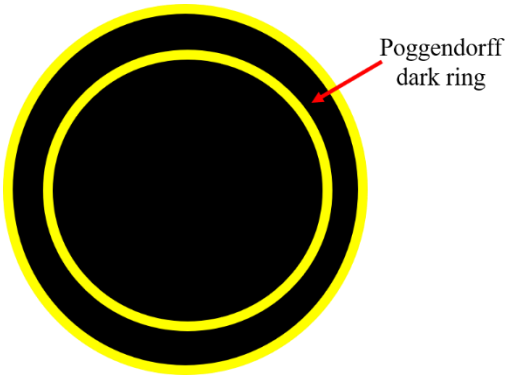

Figure 2.6: Schematic presentation of Poggendorff dark ring [7].

The plane where the light ring is observable is known as Lloyd plane, which is also called the focal image plane. After the Lloyd plane the beam then progresses to a series of rings and then evolves to an axial spike first observed by Poggendorff and Raman, respectively. Finally, the beam returns to the original profile in the far field. The Lloyd plane is also a symmetry plane [11] shown in Fig. 2.7. The center of the ring in the Lloyd plane is laterally shifted by an amount, denoted here by C, which depends on the crystal length, *l*, and a factor representing the crystal's ability for conical refraction. Voigt also reported that the lateral shift of the light cylinder observed by Lloyd depends on the orientation of the plane of optical axes of the crystal [17]. Another feature is related to the longitudinal shift of the Lloyd plane [18]. The longitudinal shift Δ, shown in Fig. 2.7, is given by

$$\Delta = l\left(1 - \frac{1}{n}\right).$$

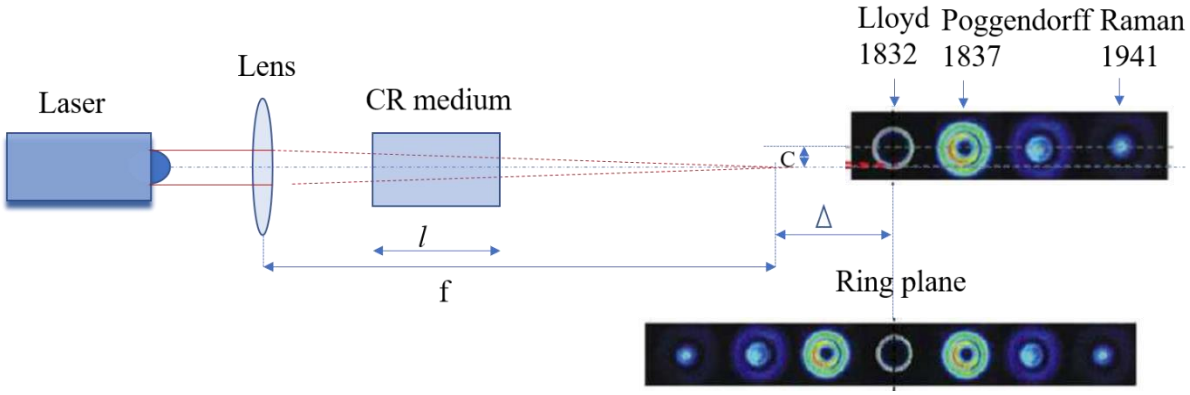

Figure 2.7: Transformation of incident Gaussian beam to conical refraction and symmetry plane [18].

In 1941 C.V. Raman reported that the transverse intensity pattern along the beam propagation direction changes: the brighter ring becomes wider and inner ring becomes a bright axial spot when imaging plane is moved further away from the Poggendorff ring plane [15] as shown in figure 2.8. Portigal and Burstein explained this phenomenon using Maxwell equations [17]

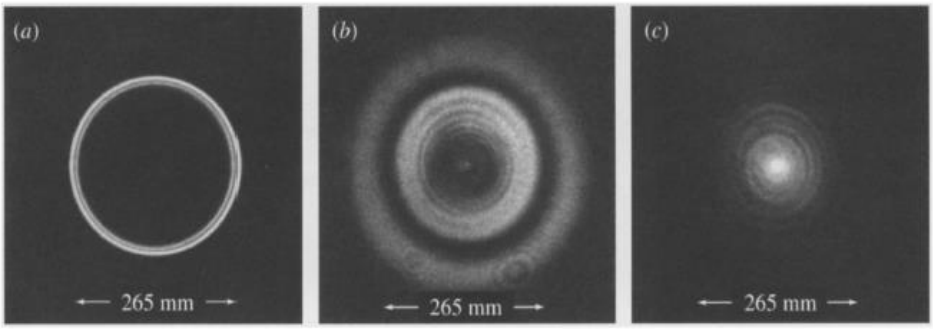

Figure 2.8: Conical diffraction patterns at increasing distances from the crystal observed by M.V. Berry et al [6].

Nevertheless, CR is not limited only to optics regime. CR has its analogues in sound waves by considering a sonic crystal. Theoretically the CR phenomenon was reported in plasma [19], honeycomb lattices [20] and Lieb lattices [21]

To generate a laser radiation using the CR phenomenon it is required to have a biaxial medium and the crystal of Nd:KGW is a suitable candidate. Therefore, its physical and optical properties have been studied in the next section.

2.2 Properties of Nd:KGW crystal

2.2.1 Physical properties

Neodymium doped Potassium-Gadolinium Tungstate crystals ($Nd:KGd(WO_4)_2$ are monoclinic in structure with and C2/c space group and are well known as Nd:KGW. Doping with lanthanides (Ln) can produce an efficient laser gain medium and it was discovered in the early seventies. This solid-state laser (SSL) medium is known for its high efficiency, low laser threshold, high doping concentration and broad bandwidth of the emission (720 GHz). It has higher stimulated emission at 1067nm in the $^4F_{3/2}$ to $^4I_{11/2}$ transition. Because of tungstate group

it has high cubic nonlinearity, $\chi^3 = 10^{-21}$ m^2 V^{-2} which means that this material is a Raman-active host with multiple emission channels [23]. Table 2.1 shows the unit-cell parameters of KGW host crystal.

Table 2.1: Unit-cell parameters of KGW.

a (Å)	b (Å)	c (Å)	β(deg)	Density of Gd^{3+} ions, N x 10^{22} cm^3	
10.652	10.374	7.582	130.80	---------	[22]
8.098	10.417	7.583	94.43	0.627	[23]

The crystallographic axes and the axes of the optical indicatrix of the KGW crystal are shown in figure 2.9. The Nd:KGW is a biaxial and anisotropic in nature along the different optical indicatrix axes named as Np, Ng and Nm. According to the schematic diagram, the Np axis and [010] direction coincide with each other and the other axes (Ng and Nm) lead by 20° and 24° from [001] and [100] directions, respectively.

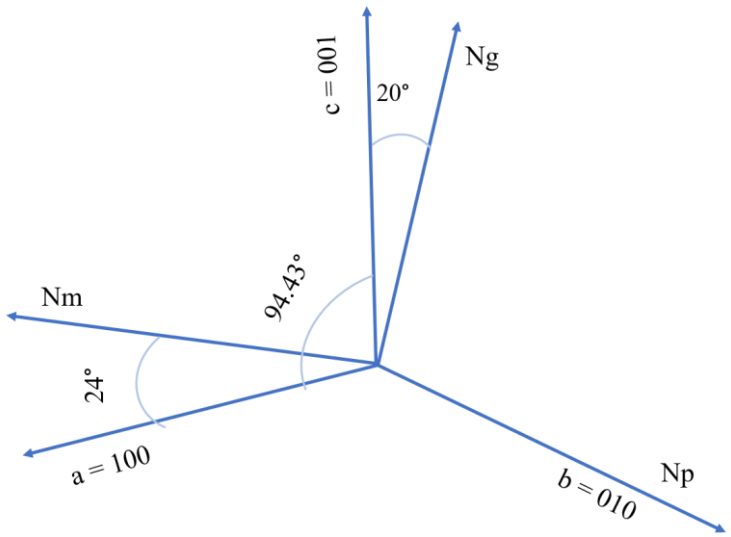

Figure 2.9: The schematic of crystallographic and the optical indicatrix axes of the KGW.

As was mentioned earlier, biaxiality is a requirement for conical refraction medium [8]. In addition, the emission, absorption and other parameters significantly vary from one axis to

another axis because of anisotropy. For laser operation KGW should be doped with active ions and lanthanide (Ln^{3+}) series ions are suitable for this task. KGW is usually doped with Nd^{3+} ions which substitute Gd^{3+}) ions. The ionic radius of Gd^{3+} (0.106 nm) is smaller than the ionic radius of Nd^{3+} (0.112 nm) and for this reason high doping concentration (up to 10 at. % [24]) is possible without any significant quenching effect. Doping ion has significant effect on the laser properties of the host material. Laser properties also depend on other physical crystal properties particularly the Poisson ratio, Young's modulus, Knoop hardness and so on. These mechanical properties are given in table 2.2 along different axes of KGW crystal. Also, the mechanical properties are affected by different parameters like heat and propagation direction.

Table 2.2: Mechanical properties of the KGW crystal [23]

Property	Value along a [100]	Value along b [010]	Value along c [001]
Knoop microhardness H (Kg/mm^2)	370	390	460
Ultimate Strength σ (Kg/mm^2)	14	10.2	6.4
Young modulus E(GPa)	115.8	152.5	92.4

Another important physical properties are thermal expansion coefficient and thermal conductivity which are highly dependent on the propagation direction. The table 2.3 shows this dependence. Low thermal expansion coefficient and higher thermal conductivity are desired qualities for an efficient laser medium. Thermal conductivity refers to the distribution of heat inside the medium. A higher the value means that the medium can transfer heat very well. On the contrary, thermal expansion is the opposite of this and it means how much the material is expanding with temperature. The principal axis of the KGW has maximum thermal expansion (α_{33} = 23.44 $x10^{-6}$ K^{-1}) [19]. When compared to other commonly used lasing media like Nd:YAG and Nd:YVO, the Nd:KGW has lower thermal expansion coefficient and it also has low thermal conductivity. Lower thermal conductivity limits the high-power operation, degrades the beam quality and stability of the laser.

Table 2.3: Temperature dependent parameter of the KGW along different axis

Property	Value along a [100]	Value along b [010]	Value along c [001]		
Thermal expansion coefficient [X 10^{-6} K^{-1} (for 100° C)]	4	1.6	8.5	KGW	[23]
	4	3.6	8.5	Nd:KGW	[25]
Thermal conductivity [$Wm^{-1}K^{-1}$ (for 100° C)]	2.6	3.8	3.4	KGW	[22]
	----	3.8	----	Nd:KGW	[25]

The damage threshold defines how much power can accumulate per unit area without damage. The table 2.4 shows damage threshold of KGW crystal along different propagation directions.

Table 2.4: Laser damage threshold of KGW crystal for τ = 20 ns, λ= 1.06 μm [22].

Propagation direction	P X 10^{10} W/cm^2		
	E ∥ Nm	E ∥ Ng	E ∥ Np
Nm		5	18
Np	17		16
Ng	16	7	

The refractive index of Nd:KGW varies along three principal axes and leads to birefringence. This plays an important role for conical refraction since the semi-angle depends on it. Table 2.5 represents the refractive indices reported by different authors. Even though they reported different values, they are not inconsistent. However, variation of temperature has significant influence on refractive indices which is known as thermo-optic coefficient and denoted as dn/dT. According to Mochalov et al. it has positive refractive index change along the Ng propagation direction [23] [25]. Furthermore, the thermo-optic coefficient (dn/dT) changes not only with the change of propagation direction but also it changes with the change of light wavelength.

Table 2.5: Refractive indices of KGW.

Property	Value along $E \parallel N_m$	Value along $E \parallel N_g$	Value along $E \parallel N_p$	
Refractive index	1.986	2.033	1.937	[23]
	2.014	2.049	1.978	[26]
	2.045	2.086	2.013	[27]

2.2.2 Spectroscopic properties

The most important spectroscopic properties include the absorption and emission spectra. There are several absorption bands for different polarizations as shown in figure 2.10 and they are highly dependent on the propagation direction of incident light. The absorption cross-section denotes the absorption capacity of a molecule for a particular wavelength and polarization. Nd:KGW has higher absorption cross-section for E || Nm polarization (26.75×10^{-20} cm^2) as compared to the other two E||Np (7.81×10^{-20} cm^2) and E||Ng (3.43×10^{-20} cm^2) polarizations. The absorption cross-section is the highest at around 810 nm for all polarizations. Also there are much lower absorption cross-sections for the wavelength of around 910 nm [10].

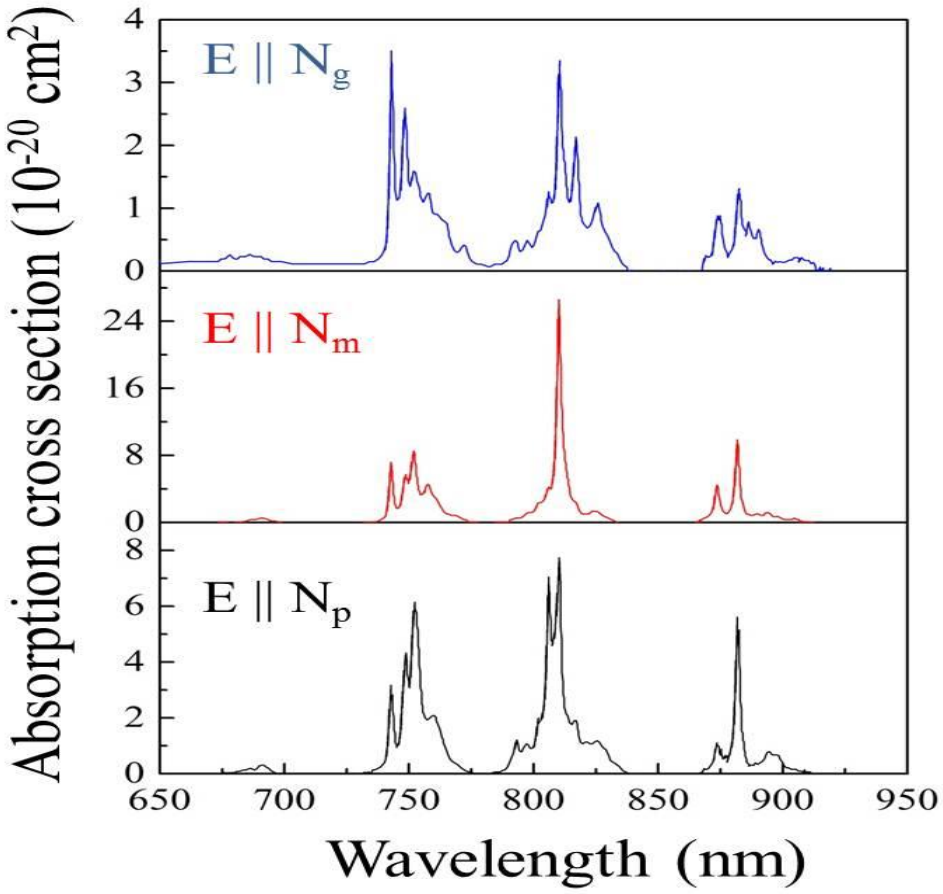

Figure 2.10: Absorption cross-sections of Nd:KGW for different polarizations [28].

Emission cross-section σ defines the emission properties of active ion. Emission cross-section plays an important role in the laser threshold pump power and the relation is P_{th} α 1/σ, where, P_{th} is the threshold pump power.

Figure 2.11 shows the polarization dependent emission cross sections at room temperature and all of them have a high gain transition at 1067 nm as compared to other transitions, but they are not equal in magnitude. In contrast, 1069 nm wavelength has higher emission cross-section for the Np polarization reported in [23]. The laser output at 1067 nm is polarized which is good for applications like non-linear optical frequency conversion such as stimulated Raman scattering or second harmonic generation [29-31]. At the same time emission at other wavelengths with lower emission cross-sections can be used for enhanced energy storage which is beneficial for generation of powerful Q-switched pulses from lasers [32].

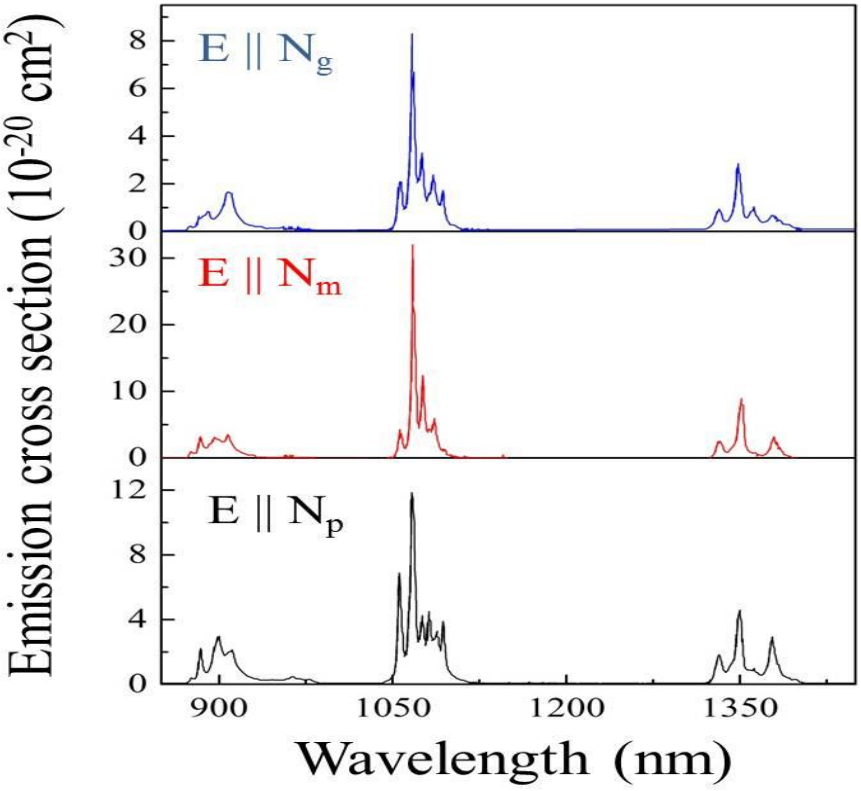

Figure 2.11: Emission cross-section of Nd:KGW for different polarization [28].

The energy level diagram of Nd:KGW is shown in figure 2.12 where only two absorption wavelengths are given because 810 nm is the most commonly used and 910 nm is the one that was introduced very recently [10]. Pumping with longer wavelength reduces thermal lensing as a result of lower heating. In case of 910 nm pump the absorption transition occurs from a thermally populated upper sublevel of the ground energy manifold $^4I_{9/2}$ directly to the upper laser energy level $^4F_{3/2}$. The main laser transition occurs from the energy level $^4F_{3/2}$ to the energy level $^4I_{11/2}$ at 1067 nm. In addition, this thesis reports a laser transition that happened at 1069 nm for 3 at % doped Nd:KGW gain medium [33].

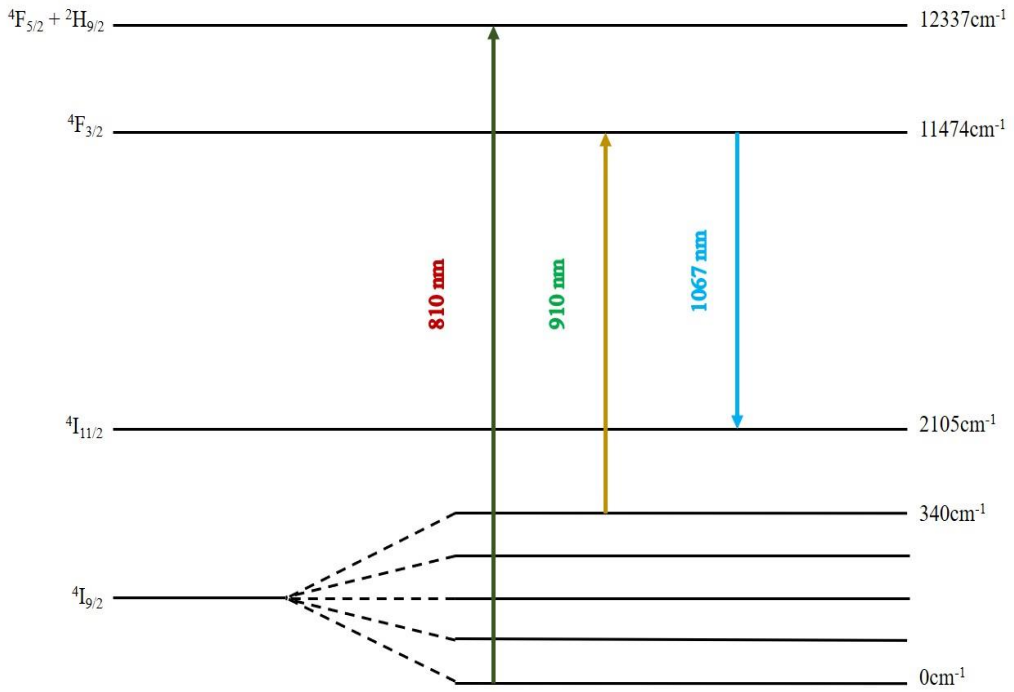

Figure 2.12: Energy level diagram of Nd:KGW laser crystal [28].

2.3 Properties of Nd:YVO_4 crystal (Vanadate)

Nd:YVO_4 (Nd:YVO) is one of the most popular laser host crystals because of its large stimulated emission cross-section, high absorption coefficient and wide absorption bandwidth at pump wavelength around 810 nm, high laser induced damage threshold, and high slope efficiency. In addition, it can produce high power infrared, green, and blue light by frequency doubling of its linearly polarized emission. Moreover this crystal has good mechanical, physical and chemical properties [34] such as Poisson ratio and Young's modulus, 0.33 and 133 GPa, respectively [35]. The lattice parameters are a = b = 7.12 Å, c = 6.29 Å and a = b = g = 90 ° means that the host material has tetragonal structure and that all of the crystallographic axes are perpendicular to each other. Figure 2.13 illustrates crystallographic axes and orientation of the crystal used in the experiment (light propagation along the a-axis).

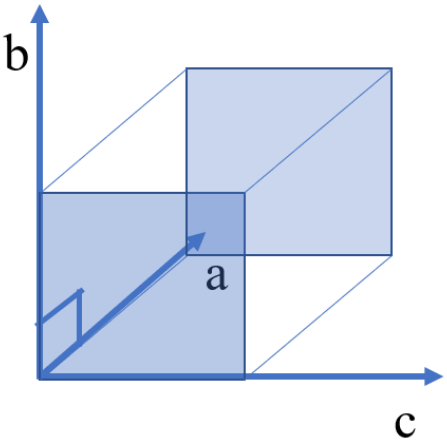

Figure 2.13: Schematic of crystallographic axes of Nd:YVO [36].

Figure 2.14 shows the absorption spectrum of the Nd:YVO for π- and σ-polarizations. The π-polarization is parallel to the optical axis (extraordinary polarization) and σ-polarization is perpendicular to the optical axis of the crystal which is generally denoted as c-axis. However, the magnitude of absorption cross section for π- polarization is approximately 4 times higher than for the σ-polarization and its maximum is at around 808 nm ($5.9 \times 10^{-19} cm^2$). Also, there is another strong absorption peak at 880 nm ($4.8 \times 10^{-19} cm^2$) as well as few other less absorbing wavelengths.

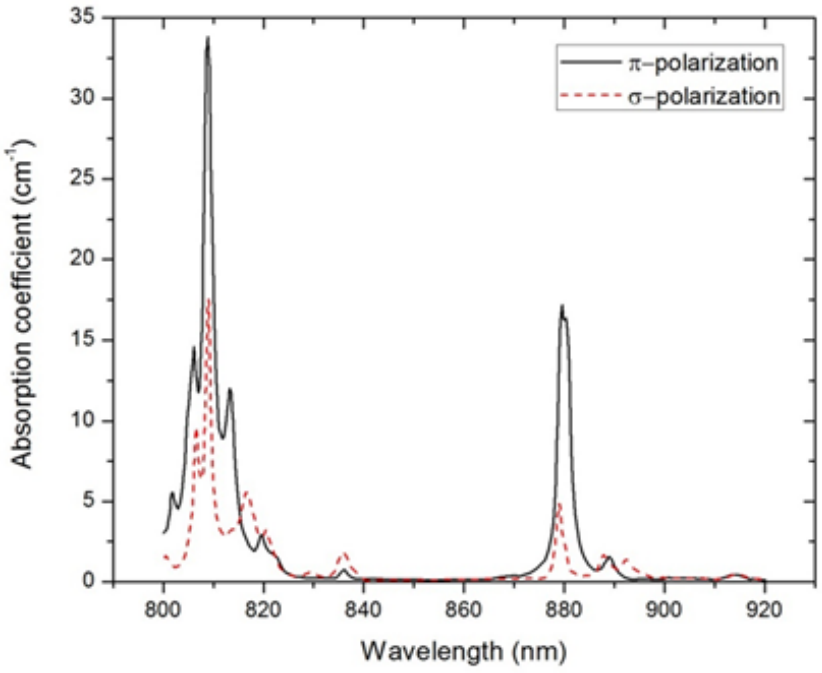

Figure 2.14: Spectrum of absorption cross-section of Nd:YVO [36].

Figure 2.15 shows the stimulated emission cross-section of the Nd:YVO for π- and σ-polarizations. The magnitude for π- polarization is approximately 3 times higher than for the σ-polarization and its maximum is at around 1064 nm (11.5 x $10^{-19}$$cm^2$). Also there are other lasing wavelengths which have very low emission cross sections as compared to the emission at 1064 nm.

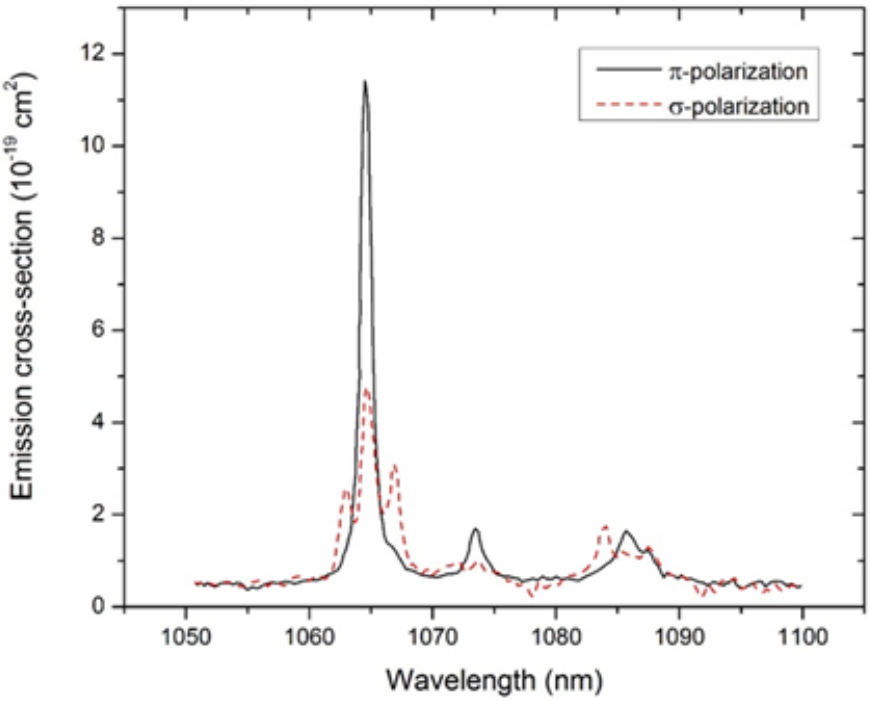

Figure 2.15: Spectrum of stimulated emission cross section for Nd:YVO [36]

The energy level diagram of Nd:YVO is shown in figure 2.16. There are multiple pump wavelengths such as 808 nm, 880 nm, 888 nm and 914 nm and there also several laser emission wavelengths at 1064 nm, 1073 nm, 1085 nm and 1342 nm. 808 nm is the most commonly used pump wavelength because of its commercially availability as well as higher absorption. Recently, 914 nm pumping also became of interest because of the available laser diodes at this wavelength and the significantly reduced quantum defect during pumping [9]. Quantum defect refers to the induced heat inside the laser crystal because of the energy loss between the absorbed and emitted photons (see fig 2.12).

Lasing at 1064 nm is a four-level system. Pump transition at 914 nm occurs from thermally populated upper sublevel of the ground manifold $^4I_{9/2}$ to the upper laser level $^4F_{3/2}$. The laser transition at 1064 nm occurs from the energy level $^4F_{3/2}$ to the energy manifold $^4I_{11/2}$.

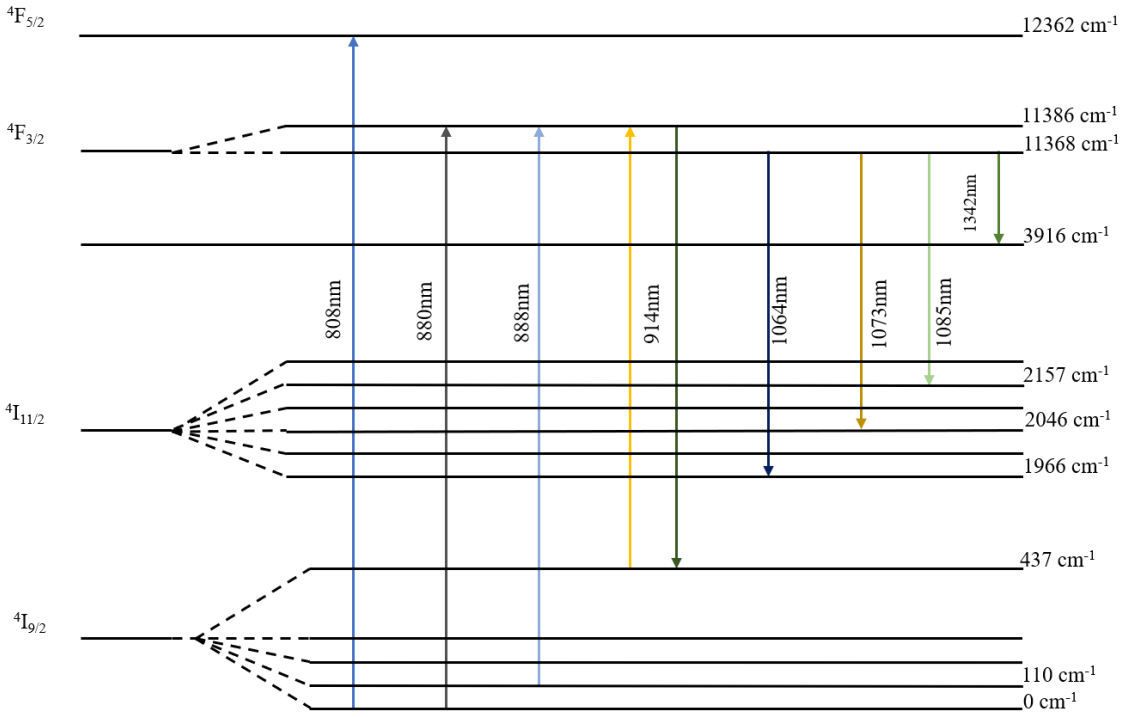

Figure 2.16: The diagram of energy levels of Nd:YVO laser gain medium [36].

The spectral and physical properties of Nd:KGW and Nd:YVO are given in the table 2.6 along with the other commonly used laser crystal [ALPHALAS GmbH]. It is obvious that Nd:YVO has lower fluorescence lifetime which is good for mode-locked operation. As compared with Nd:KGW, is has higher thermal conductivity which can help to produce higher output power level. This moment encouraged us to use Nd:YVO as a laser gain medium for passive CR laser which will be discussed in Chapter 4.

Table 2.6: The spectral and physical properties of Nd:KGW , Nd:YVO, Nd:GVO, Nd:YAG crystals.

Laser crystal type	$Nd:YVO_4$	$Nd:GdVO_4$	Nd:YAG	Nd:KGW
Lasing λ nm	914, 1064, 1342	912.6, 1063.1 1341.3	946, 1064 1319	911, 1067.2 1351
Emission cross section, X $10^{-19}cm^2$	25 @ 1064nm	7.6 @1063.1nm	2.8 @1064nm	4.3 @1067.2 nm
Fluorescence lifetime[μs] @doping	90@1%	95@1%	230@1%	110@3%
Gain bandwidth [nm]	0.96 @1064nm	0.8@1064nm	0.6 @1064nm	2.73
Pump λ nm	808.5, 910	808.4	807.5	811, 910
Absorption coefficient [cm^{-1}] @ doping 1%	31.4 @810 nm (π, e)	74.0 @810 nm (π, e)	7.1 @810 nm	4.5
Absorption line width [nm]	4 (π, e)	3 (π, e)	1	12
Polarized emission	(π, e) || c	(π, e) || c	no	polarized
Thermo-optic coefficient dn/dt [$10^{-6}K^{-1}$]	3.0 (π,e) 8.5 (σ,o)	4.7(π, e)	7.9	-0.8(p[gg]p) -5.5(p[mm]p)
Thermal conductivity [W/mK]	|| c:5.23 ⊥ c: 5.10	⊥ c:11.7	14	2.8[100] 2.2[010] 3.5[001]
Thermal expansion coefficient [$10^{-4}K^{-1}$]	$\alpha_a = 4.43$ $\alpha_c = 11.37$	$\alpha_a = 1.5$ $\alpha_c = 7.3$	7.8 [111]	4.0 [100] 3.5 [010] 8.5 [001]

2.4 Previous work on CR as well as CR lasers

In 2010 the first Nd:KGW conical refraction laser was demonstrated with 808 nm pumping and produced 3.3W of output power at 1067 nm with slope efficiency as high as 74% [18]. A. Abdolvand et al. also reported cascaded conical refraction system where output beam was identical to the original input beam, i.e. intermediate CR beam was converted back to the Gaussian.

Later K.G. Wilcox et al. reported Nd:KGW laser which could generate Gaussian and conically refracted laser beams simultaneously. The laser was pumped at 808 nm and produced 530 mW of output power at 1067 nm with 30% slope efficiency [37].

In 2014 a holmium-doped $KY(WO_4)_2$ crystal (a sister material to KGW) was pumped at 1960 nm and obtained 1.6W of CR laser radiation at 2074 nm with 52% slope efficiency. The output beam of this CR laser displayed a crescent shaped beam profile [38].

On a passive CR side, focused input beam that splits into two cones after conical refraction has been recently demonstrated [39]. [40]. In addition CR has the capacity to restore the input beam after passing through the 180° rotated another CR medium or when it is reflected back [40]. [18]. There were also several other researchers who observed the passive CR and examined its different properties [1-3]. [41].

Chapter 3: Experimental setup

3.1 Laser cavity design

To design an optical cavity, we need primarily to focus on cavity stability and its mode size in the crystal. Cavity mode size is important because a good overlap between the pump and the cavity modes is required to achieve an efficient laser operation. There is a commercially available software to design laser cavity considering all these facts. In my case, the optical cavity was designed by using the reZonator software. This software package uses the ABCD matrix analysis technique for cavity design. The final ABCD matrix is the multiplication of optical matrices of all element's that comprise the cavity. This ABCD matrix also denotes the freedom for choosing the properties of individual elements if it fulfills the stability condition given as

$$-1 \leq \frac{A+D}{2} \leq 1 ,$$

where ABCD matrix = $\begin{bmatrix} A & B \\ C & D \end{bmatrix}$.

3.1.1 Three-mirror cavity

Figure 3.1 shows the 3-mirror cavity design where M1 represents a flat dichroic mirror which has 100% transmission at the pump wavelength and 100% reflection at the lasing wavelength. The L1, L3, L4 define the air gaps between the elements which have the refractive index of 1. The M_out indicates the flat output coupler (OC) which transmits only a portion of laser light out of the cavity. The M_2 is the cavity focusing mirror which is treated as a lens in simulations.

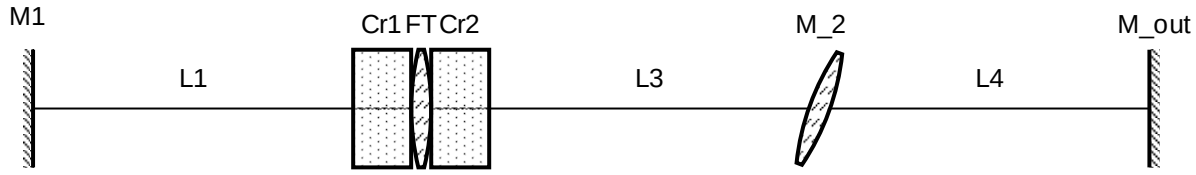

Figure 3.1: Schematic diagram of equivalent laser cavity designed in simulator.

In our case the M_2 is the equivalent lens of a 500 mm radius of curvature concave mirror which is 100% reflective at the laser wavelength. The Cr1 and Cr2 represent the two halves of the laser crystal and FT represents the thermally induced lensing effect. The total length of the used Nd:KGW crystal was 18 mm and of designed cavity around 880 mm.

Table 3.1: The parameters used to design a laser cavity in the reZonator software.

Description	Label	Parameter
Flat dichroic mirror	M1	Pump T=98%
Air gap	L1	L=24 mm
1st half of laser crystal	Cr1	L = 9 mm, n = 2.049
Thermal lens	FT	F = 200 mm, Alpha = 0°
2nd half of laser crystal	Cr2	L = 9 mm, n = 2.049
Air gap	L3	L = 398 mm
Focusing curve mirror	M_2	R = 500 mm, Alpha = 5°
Air gap	L4	L = 439 mm
Flat output coupler	M_out	T = 1.6%, 2.4%, 5%

The ABCD matrix at the output coupler was calculated using the reZonator and the results are given below:

ABCD = M_out * L4 * M_2 * L3 * Cr2 * FT * Cr1 * L1 * M1 * L1 * Cr1 * FT * Cr2 * L3 * M_2 * L4

$$M_T = \begin{bmatrix} 0.83 & -259.54 \\ 0.001 & 0.83 \end{bmatrix};$$

$$MS = \begin{bmatrix} 0.815 & -276.382 \\ 0.001 & 0.815 \end{bmatrix}$$

Where M_T and M_S refer to tangential (horizontal) and saggital (vertical) roundtrip matrices.

The pump mode size radius was 275 µm at the crystal, so we needed to find the beam radius of 275 µm at the crystal after one round trip. In this case the ρ_0 is 1.11 for the CR effect. The beam radius is shown in the figure 3.2 which starts at dichroic mirror and ends at the output coupler. A condition for a stable laser cavity is that the laser beam should repeat itself after one round trip.

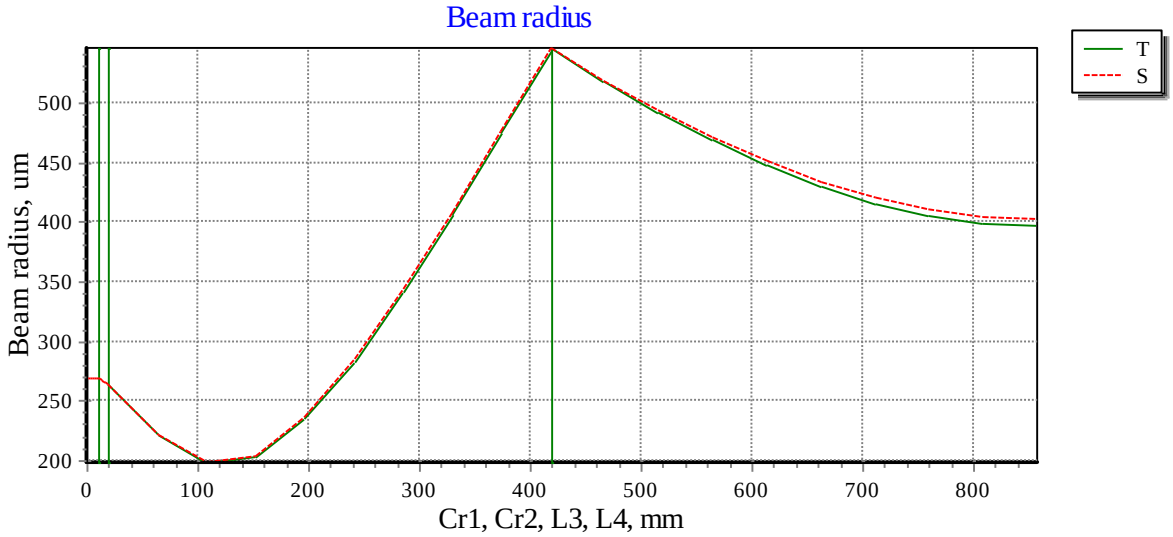

Figure 3.2: Simulated beam radius in the laser cavity.

Thermal lensing significantly affects the beam radius at the output coupler. The figure 3.3 shows the changes of the beam radius for the thermal lens focal lengths between -300 mm and 250 mm. Such a change could make the cavity unstable (e.g. in the -250 to 150 mm range of focal lengths).

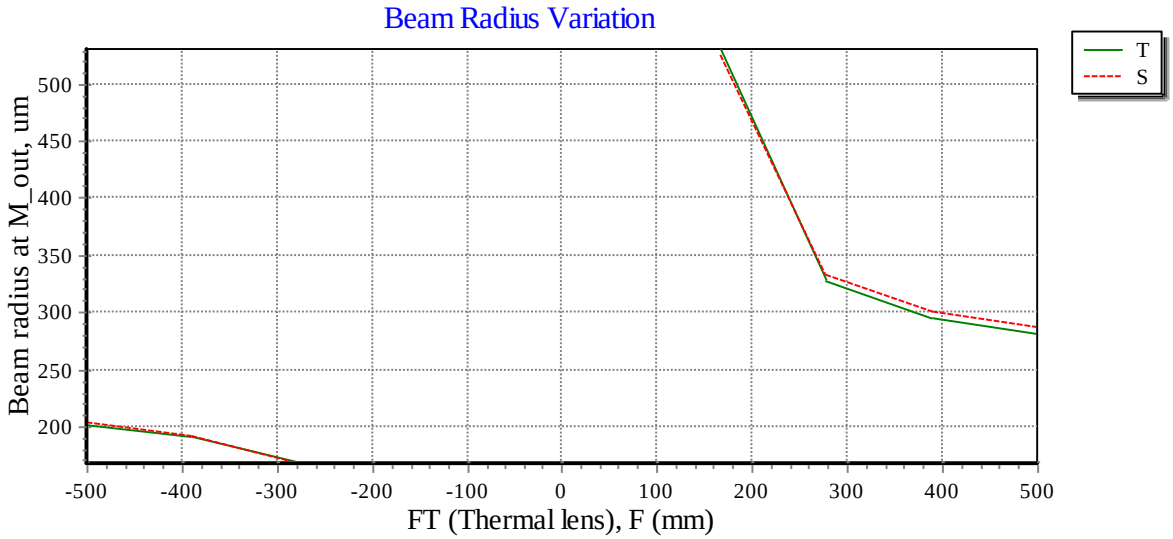

Figure 3.3: Simulated thermal lensing effect on the beam radius.

Figure 3.4 illustrates the simulated result of how the stability parameter depends on the focal length of the induced thermal lens. It is obvious that the cavity is unstable for the focal length of less than approximately -180 mm up to to 24 mm and from 45 mm to 160 mm. Any other

focal length of the thermal lens will lead to a stable cavity. Unstable cavity defines the laser beam that will not be confined within the cavity and for a stable cavity it is vice versa.

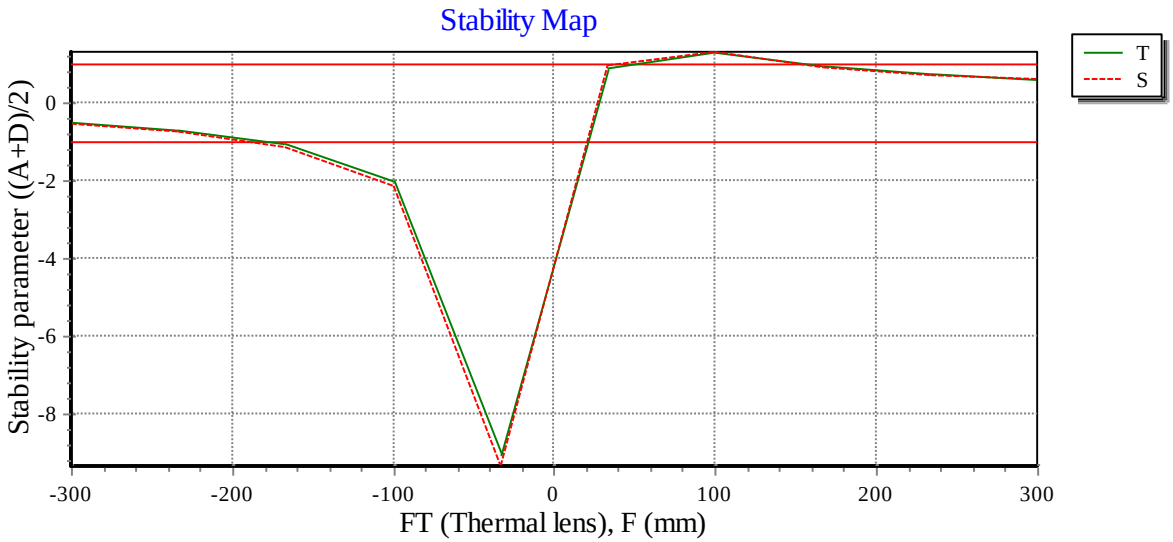

Figure 3.4: Simulated result of stability dependence on the focal length of thermal lens.

3.1.2 Four-mirror laser cavity

In active CR laser setup, the mode size inside the crystal was quite large and it didn't fulfill the condition to observe a clear CR pattern. Also the Nd:KGW has inferior thermal conductivity. To overcome these issues, we designed another experiment which used a different laser cavity. In this case laser action was produced by a Nd:YVO crystal and the CR was produced by the Nd:KGW crystal. This allowed us to set the mode sizes in both crystals separately. The figure 3.5 shows the 4-mirror cavity design where M2 represents a flat dichroic mirror. The L1, L3, L4, L5 define the air gaps between the elements and M_out indicates the flat OC. The M_2 is the equivalent lens of a 500 mm radius of curvature mirror. Another important element is the focusing mirror M1 with radius of curvature of 400 mm. It focused the laser beam coming from the M_2 into a smaller beam waist inside the CR crystal (Nd:KGW) to produce a CR pattern. The beam radius inside the CR crystal was around 150 µm and it made a larger ρ_0 of 2.04 in comparison with pervious cavity design. A large ρ_0 is one of the requirements to get a clear CR pattern. The total cavity length was around 985 mm.

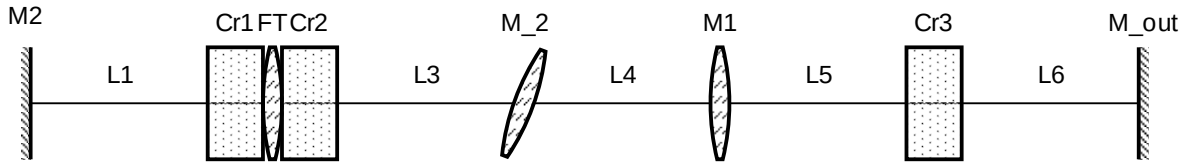

Figure 3.5: Schematic equivalent of a 4-mirror laser cavity.

Table 3.2: The parameters used to design a laser cavity in the reZonator software.

Description	Label	Parameter
Flat dichroic mirror	M2	Pump T=98%
Air gap	L1	L=24 mm
1st half of laser crystal	Cr1	L = 10 mm, n = 2.17
Thermal lens	FT	F = 200 mm, Alpha = 0°
2nd half of laser crystal	Cr2	L = 10 mm, n = 2.17
Air gap	L3	L = 398 mm
Focusing curve mirror	M_2	R = 500 mm, Alpha = 5°
Air gap	L4	L = 370 mm
Focusing curve mirror	M1	R = 400 mm, Alpha = 0°
Air gap	L5	L = 150 mm
CR crystal	Cr3	L = 18 mm, n = 2.049
Air gap	L6	L = 6 mm
Flat output coupler	M_out	T = 1.6%, 5%

The ABCD matrix at the output coupler was calculated using the reZonator software and is given below

ABCD = M_out * L6 * Cr3 * L5 * M1 * L4 * M_2 * L3 * Cr2 * FT * Cr1 * L1 * M2 *

L1 * Cr1 * FT * Cr2 * L3 * M_2 * L4 * M1 * L5 * Cr3 * L6

$$M_T = \begin{bmatrix} 0.046 & 64.464 \\ -0.015 & 0.046 \end{bmatrix}$$

$$M_S = \begin{bmatrix} 0.072 & 63.51 \\ -0.016 & 0.072 \end{bmatrix}$$

The pump and cavity mode size matching is also applicable here to achieve higher efficiency. As we used the same pump, the cavity mode size radius was around 275 µm at the crystal after one round trip. Beam radius is shown in the figure 3.6. It starts at the dichroic mirror and ends at the output coupler.

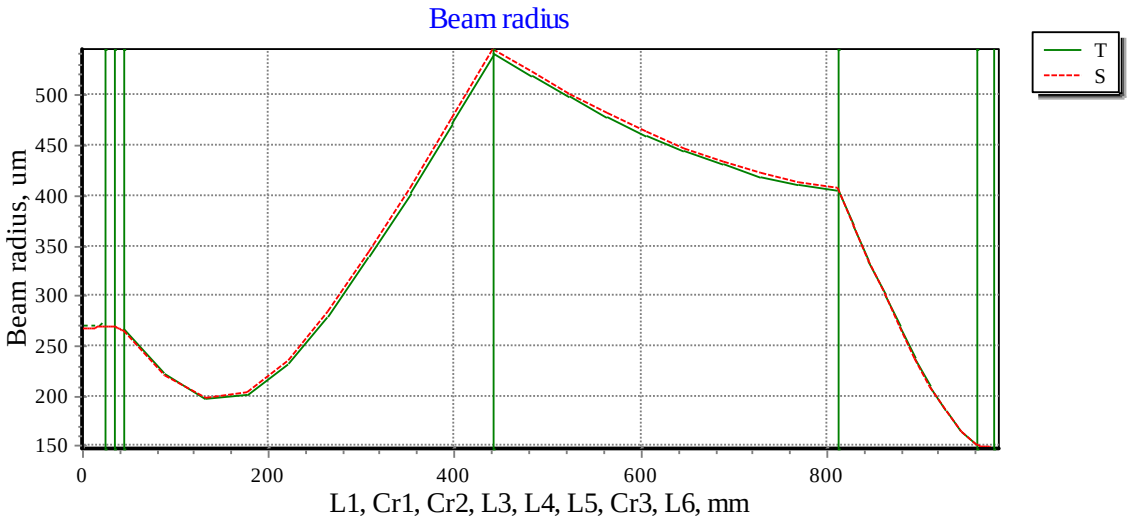

Figure 3.6: Simulated beam radius in the 4-mirror laser cavity.

In this design the beam radius gradually increased at the output coupler with the positive values of focal length of the induced thermal lens. Below the focal length of 100 mm the cavity quickly becomes unstable. Figure 3.7 shows the beam radius changes with the change in focal length of thermal lens.

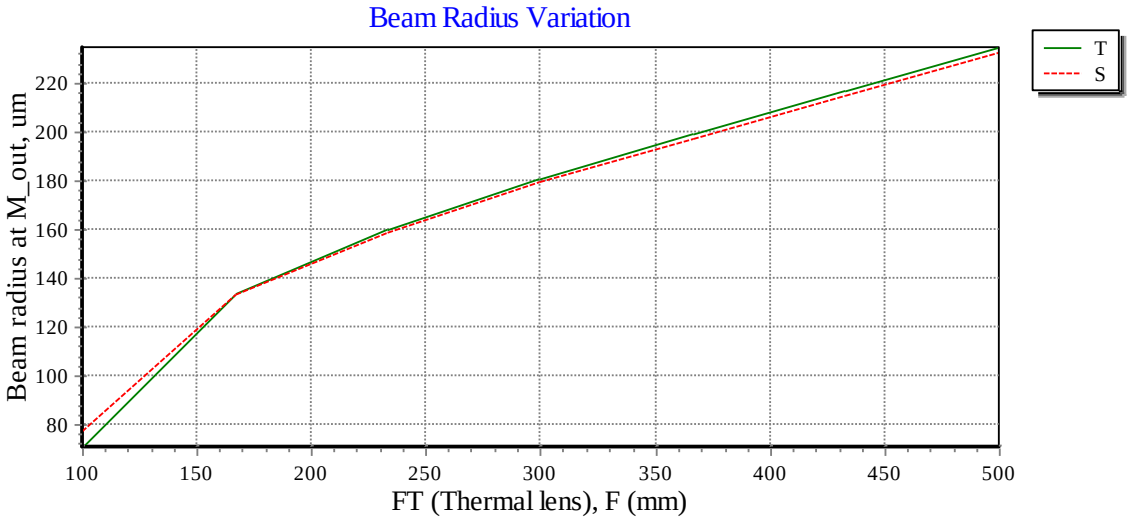

Figure 3.7: Simulated thermal lensing effect on the beam radius.

Figure 3.8 shows the simulated result of how the stability parameter depends on the focal length of thermal lens. Its shows that the cavity is stable for the focal lengths between 50 mm and 800 mm and for any other focal lengths the cavity will be unstable.

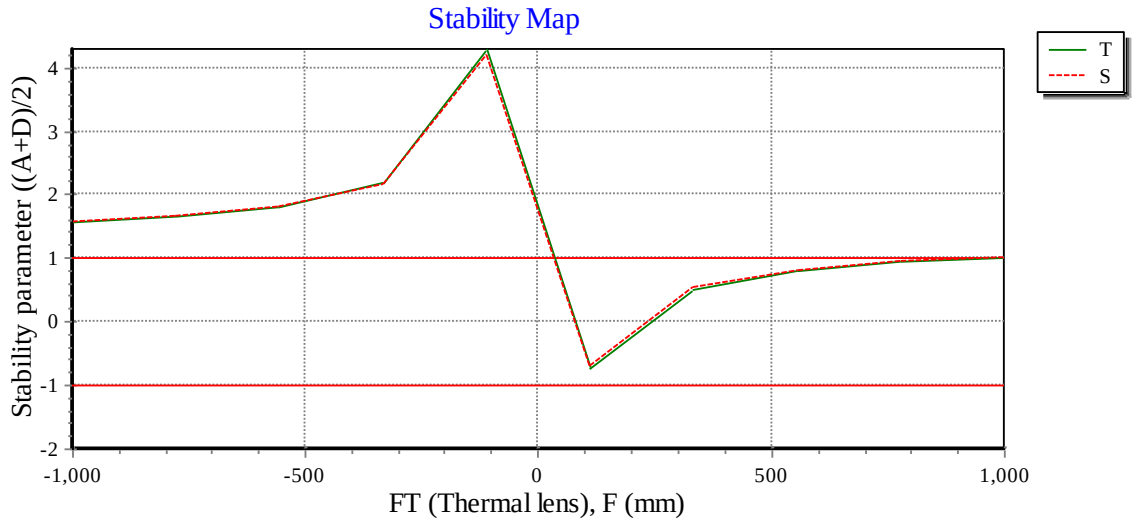

Figure 3.8: Simulated result of stability dependence on the focal length of thermal lens.

3.2 Experimental Setup

3.2.1 Pump diode

The pump laser diode was cooled using a thermoelectric cooler (Model CP - 061) and its temperature was kept constant at 25.6°C by a digital temperature controller.

The crystals of Nd:KGW and Nd:YVO have been pumped by using a high power fiber-coupled laser diode operating at 910 nm which produced unpolarized light out of the fiber. The fiber had a core diameter of 105 μm and a numerical aperture of 0.22. The laser light was collimated with a lens with focal length of 40 mm and subsequently focused onto the laser crystal using another lens with 200 mm focal length. This produced a pump spot radius of 275 μm. Figure 3.9 shows the laser diode spectrum which was observed using an Ocean Optics HR4000 spectrometer.

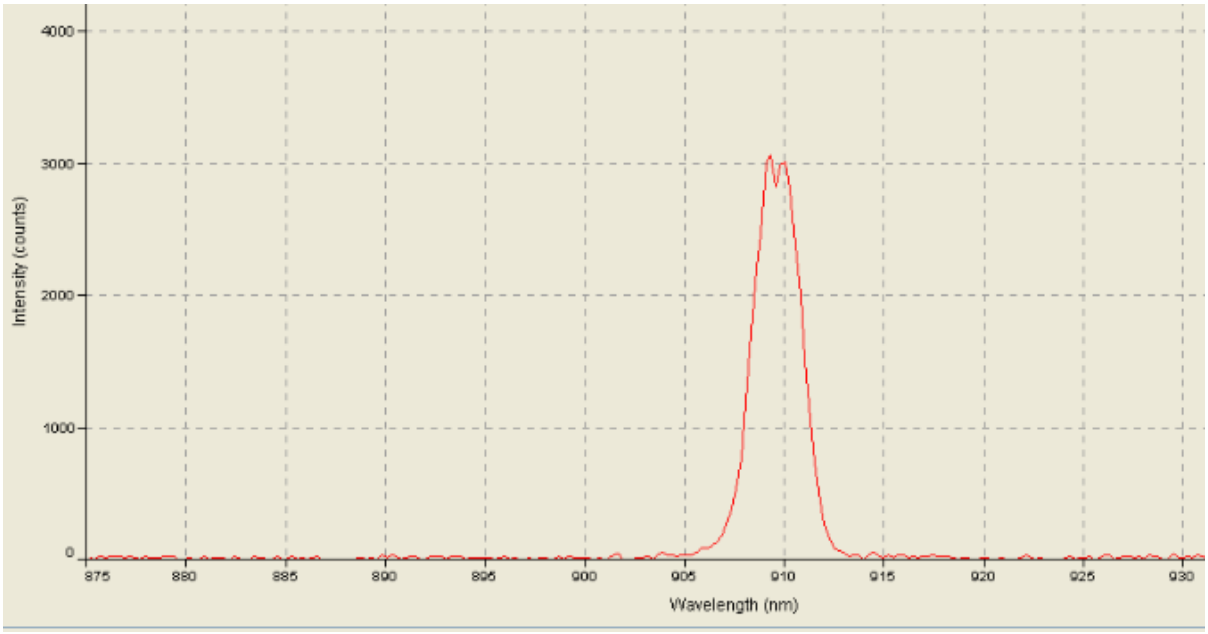

Figure 3.9: Spectrum of pump laser diode.

As was mentioned, high power operation is limited by the thermal properties of the used laser crystal. Thermal gradient is the result of heat generation inside of the laser crystal due to the quantum defect. Quantum defect is defined as the difference in pump and laser photons energies:

$E_{QD} = E_{pump} - E_{laser}$

$$E_{QD} = hc\left(\frac{1}{\lambda_{pump}} - \frac{1}{\lambda_{laser}}\right),$$

where

E_{QD} = Quantum defect

E_{pump} = Energy of the pump photon

E_{laser} = Energy of the laser photon

λ_{laser} = Wavelength of laser radiation

λ_{pump} = Wavelength of pump radiation

c = Speed of light

It is clear from the above equation that the larger the difference between the pump and laser wavelengths the larger will be the quantum defect and hence the heat deposition in the crystal. We can overcome this problem by pumping the laser crystals at 910 nm instead of conventional 808 nm.

3.2.2 Experimental setup of passive CR

A simple setup was made to check that the available 18 mm-long Nd:KGW crystal can work as conical refraction medium. The setup used a collimated laser, focusing lens, CR crystal and a CCD camera. A He-Ne laser at 633 nm was used as a light source and a convex lens with 125 mm of focal length was used to focus the laser light into the crystal. The crystal must be placed before the focal length of the lens in order to observe the CR ring. The crystal was placed 30 mm from the lens and the CCD was placed 79 mm from the exit face of the crystal. Since for our laser crystal the calculated ring radius of the CR pattern was 306 µm, this setup had the ratio (ρ_0) between the CR ring radius and the beam waist radius of about 4.5. The position of the CCD was not at the focal spot because the ring plane has a small shift along the propagation direction as discussed in section 2.1 of Chapter 2. Figure 3.10 illustrates the schematic diagram of the experimental setup for observation of passive conical refraction.

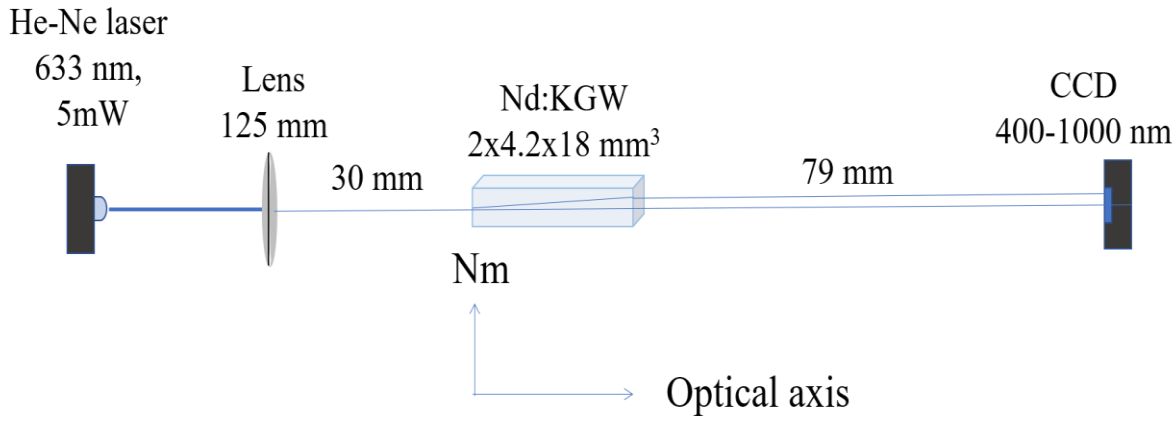

Figure 3.10: Schematic diagram to observe conical refraction.

3.2.3 Experimental setup of active CR laser

Figure 3.11 shows the schematic diagram of a laser cavity containing the Nd:KGW gain medium which was cut along one of the optical axes to get CR [19] and the optical axis was located in the Ng-Np plane. The crystal dimensions were 2x4.2x18 mm^3, it had 3at% Nd-ion doping, and was antireflection coated at the laser and pump wavelengths. The crystal was wrapped in indium foil and held by a water-cooled (16° C) metallic holder. A dichroic mirror

(DM) was used to introduce the pump light at 910 nm into the cavity which was designed taking into account thermal lensing [42]. L1, L2 and L3 distances were 24 mm, 398 mm and 439 mm, respectively, and produced a beam diameter of 550 μm in the crystal. M1 was a concave mirror (r=500 mm) and the output coupler (OC) had 2.4% transmission at the laser wavelength.

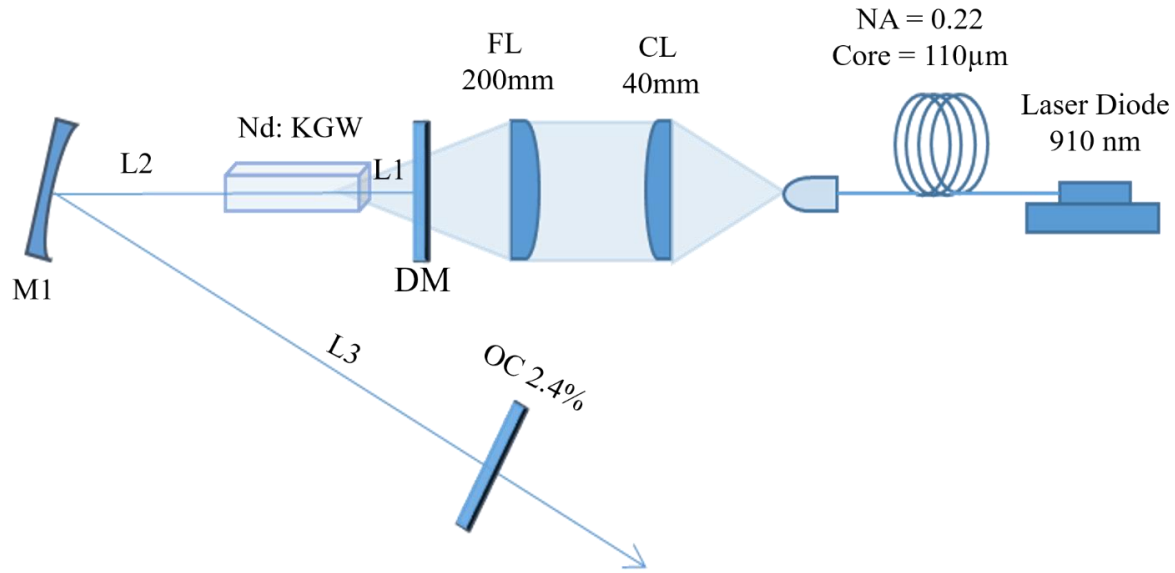

Figure 3.11: Schematic diagram of CR Nd:KGW laser (active CR).

A red He-Ne laser was used to observe a conical refraction ring pattern at the plane of the DM using a CCD camera. The propagation direction of the He-Ne laser was aligned to be collinear with the generated laser light, thus ensuring alignment close to the CR condition.

3.2.4 Experimental setup of passive CR laser

As was mention earlier in section 3.1.2, there was a limitation of mode spot size in the 3-mirror cavity active CR laser. Because the mode size inside the laser crystal was around 275 μm, it was far too big to fulfill the condition of producing the CR pattern. In addition the Nd:KGW has lower thermal conductivity that limits the laser to operate in high power regime. To overcome this difficulty as well as to enable further power scaling we introduced the 4-mirror cavity for passive CR laser. Figure 3.12 demonstrates the schematic diagram of passive conical refraction laser where Nd:YVO crystal was used as a laser gain medium and the Nd:KGW crystal was used as a conical refraction medium. The Nd:YVO crystal dimensions were 2x3x20 mm^3, it had 1.5at% Nd-ion doping, and was antireflection coated at the laser and pump wavelengths. The pumping procedure as well as crystal cooling were the same as previously

described for the active conical refraction experiments. L1, L2, L3 and L4 distances were 24 mm, 398 mm, 370 mm and 174 mm, respectively, and produced a beam diameter of 550 µm in the crystal as before. M1 and M2 were concave mirrors (r=500 mm and r = 400mm, respectively) and the output coupler (OC) had 1.6 % or 5% transmission.

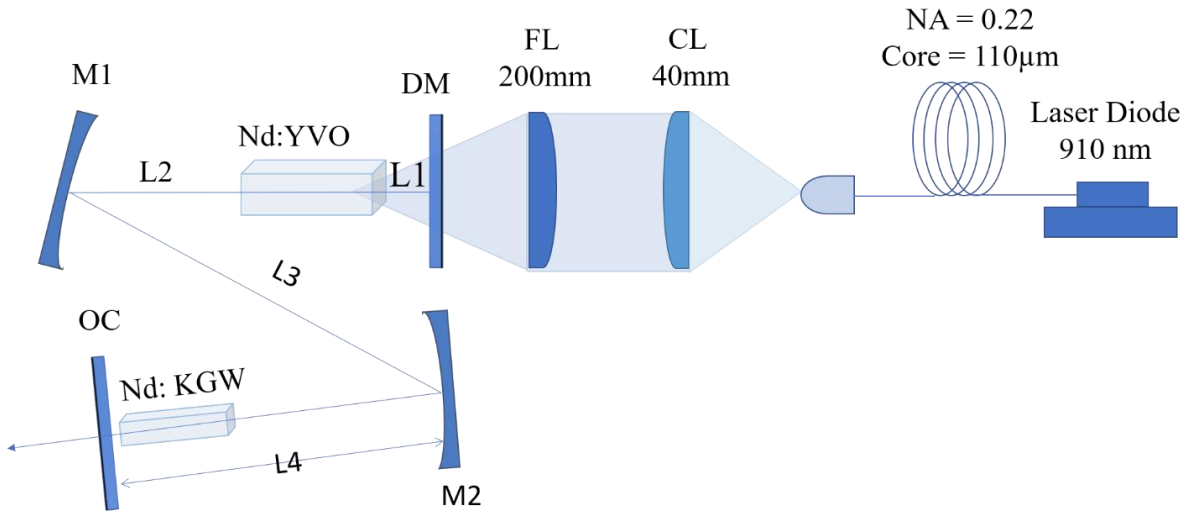

Figure 3.12: Schematic diagram of passive conical refraction laser.

The Nd:KGW crystal was placed close to the OC to observe the CR pattern. The output beam was imaged onto a CCD camera. The beam radius was around 200 µm at the entrance of the Nd:KGW crystal. Since the Nd:KGW does not absorb the lasing wavelength of 1067 nm it did not require cooling. At the OC the laser power was too high for the CCD camera to handle and for this reason we used additional supporting setup. It included a dichroic mirror to eliminate the residual (unabsorbed) pump from the produced laser radiation and additional 1.6% OC to decrease the laser power to make it tolerable for the CCD camera. A lens with 125 mm of focal length was used to image the output laser beam at the OC onto the CCD camera.

Chapter 4: Results and discussion

4.1 Observation of the CR pattern

A He-Ne Red laser (HRP 050-1) with 5 mW output was used as a coherent light source to observe the CR ring in the setup described in section 3.2.2. The beam was attenuated with a neutral density filter and focused by a 125 mm focal length lens. The Nd:KGW crystal was placed such that the focal spot occurred after it. A charged coupled device (CCD) was placed after the crystal to observe the CR ring. In addition, a number of different neutral density (ND) filters has been used in front of the CCD to reduce the intensity of the laser beam in order to avoid saturation of the CCD camera. Besides these, the most important factor in the experiment was alignment of the Nd:KGW crystal to ensure laser light incidence along one of the optical axes of the crystal. At the proper alignment we have observed the ring and the figure 4.1 shows how the ring was formed starting from the misaligned (left picture) to the aligned position (right picture). The ring plane was after the focal point which is in good agreement with the previously reported experiment [18].

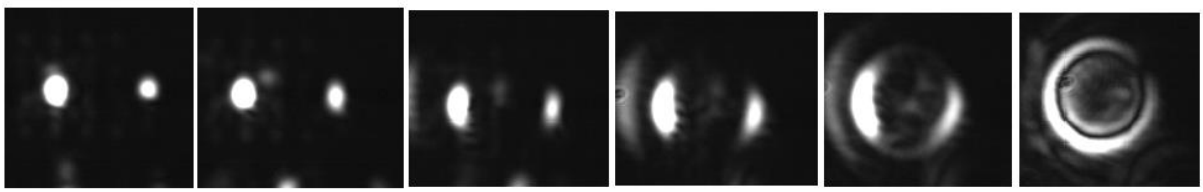

Figure 4.1: CR ring formation by changing the alignment of the Nd:KGW crystal. Left – misaligned, right – aligned.

Furthermore, after the ring plane the inner ring evolved to a central spot in the far field. However, the conical ring would not be formed without the focusing lens because the beam diameter of He-Ne laser was too large. The ring was not complete because the input beam was linearly polarized. Other bright spots in the image were caused by the reflections from the ND filters in front of the CCD camera.

We also observed the CR pattern for different values of ρ_0 (ratio of the CR ring radius to the incident beam waist) and confirmed that to get a sharp CR ring pattern the incident beam waist

must be small enough as predicted by theory. Figure 4.2 shows the ring pattern for different values of ρ_0.

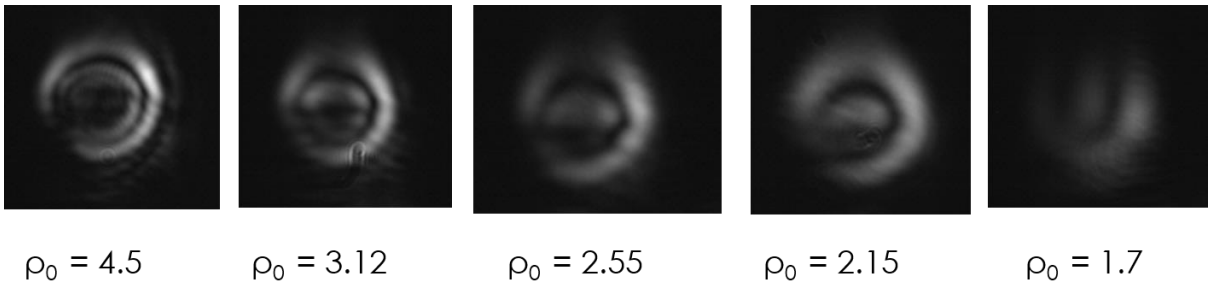

Figure 4.2: Observed CR patterns with He-Ne laser for different values of ρ_0.

4.2 Observation of active CR Nd:KGW laser

A 3-mirror laser cavity described in section 3.2.3 (with the Nd:KGW crystal) could operate in the CR laser mode as well as in the normal non-CR regime with a careful adjustment of cavity mirrors. A transition between these two regimes was accompanied by the change in the position of the generated laser mode at the DM (dichroic mirror). In addition, in the non-CR regime lasing took place at 1067 nm and in the CR regime - at 1069 nm. In both cases the laser had an excellent beam quality. Figure 4.3 shows the beam profile and the spectrum of the laser wavelengths. A similar dual wavelength operation of a CR laser was also observed by Alain Brenier [1].

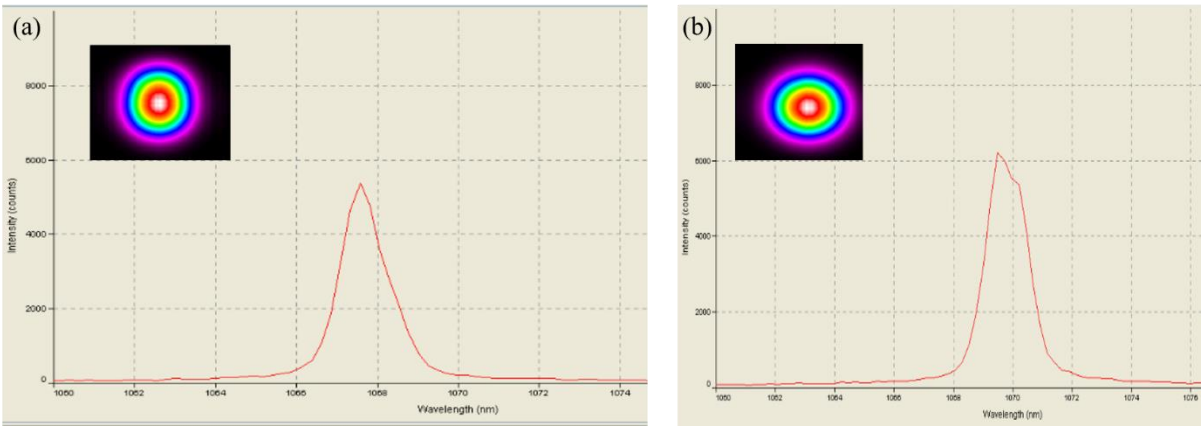

Figure 4.3: Laser spectrum and corresponding beam profile at a) 1067 nm and b) 1069 nm.

At the wavelengths of 1067 nm and 1069 nm the Nd:KGW laser produced maximum output powers of 1.8 W and 1.15 W, respectively, using 2.4% output coupler. We also tried the 1.6% and 5% output couplers but the 2.4% was found to produce higher output powers. The threshold pump powers were measured to be 0.55 W for 1067 nm and 1.52 W for 1069 nm lasing. Lower output power as well as higher threshold pump power in the CR regime can be explained by the laser beam walk-off (which reduced pump-mode overlap) and agrees with the previous report [38]. The output beam did not produce the CR ring pattern in the current setup due to a big mode size in the crystal (ρ_0 = 1.11 for a 275 μm beam). Figure 4.4 shows the output power versus the absorbed pump power for both regimes with the slope efficiencies of 46% and 32% and optical to optical efficiencies of 40.1% and 25.6% for 1067 nm and 1069 nm lasers, respectively. The slope efficiency represents the rate of change of the output power with respect to the pump power. Optical to optical efficiency represents the ratio of maximum output power to the corresponding absorbed pump power value. This can be compared with the recently reported non-CR Nd:KGW laser pumped at 910 nm which had a slope efficiency of 43 % and optical to optical efficiency of 35% at the laser wavelength of 1067 nm [10]. On the other hand, among the CR Nd:KGW lasers our slope efficiency was higher when compared with the work of K.G.Wilcox et al. (30 %) [37] and our optical to optical efficiency was lower than in the work by Y. V. Loiko et al. (30 %) [40]. At the same time R. Cattoor et al. reported a Ho:KYW CR laser with slope efficiency of more than 50%. Although A. Abdolvand et al. had the highest slope efficiency, but there was no CR pattern observed in the experiment. Table 4.1 accumulates few previously reported results on CR Nd:KGW lasers and gives a comparison with our work.

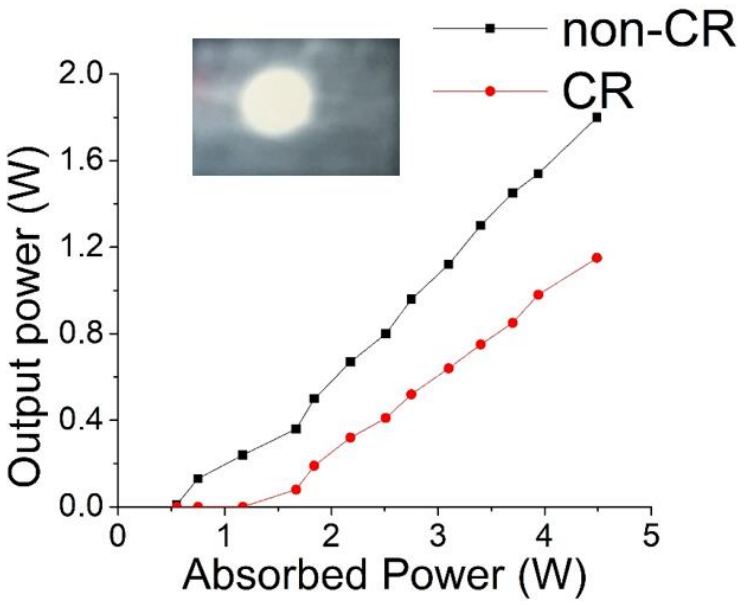

Figure 4.4: Output power vs the absorbed pump power for both the CR and non-CR Nd:KGW laser.

Table 4.1 Previous reported results on CR Nd:KGW lasers.

Author	Pump λ (nm)	CW output power (W)	Slope efficiency (%)	Opt-to-opt efficiency (%)	Cavity mirrors	Year
A. Abdolvand et al.	808	3.3	74	66	2	2010
Y.V. Loiko et al.	805	-----	-----	30	2	2014
A. Brenier	810	0.015	-----	-----	2	2016
This work	910	1.8	46	40.1	3	2017

4.3 Observation of passive CR laser with Nd:KGW crystal

A four-mirror cavity was designed (see section 3.2.4) which incorporated both a 1.5 at % Nd:YVO4 crystal as well as the Nd:KGW crystal element. According to my knowledge, this type of arrangement for a CR laser was introduced for the first time. Nd:YVO crystal performed

as a laser gain medium and the Nd:KGW crystal acted as an intracavity CR medium. It was placed very close of the output coupler. Please recall that it is required to have a smaller beam waist at the entrance of a CR medium as compared to the CR ring radius supported by the crystal in order to observe a clear CR pattern (i.e. $\rho_0 >> 1$) [6]. Experimentally measured beam waist at the position of the output coupler (and hence at the Nd:KGW crystal) was around 200 µm (vs simulated waist radius of 150 µm) . Since the theoretical CR ring radius was 306 µm for our crystal, the ρ_0 was 1.53. We aligned the Nd:KGW crystal so that the incident laser beam could propagate parallel to the optical axis using a He-Ne laser. Figure 4.5 shows the ring shape that we obtained from the alignment laser.

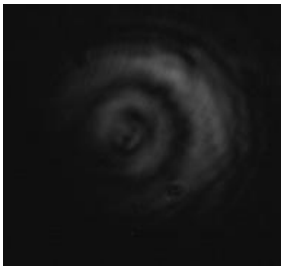

Figure 4.5: CR ring obtained after the output coupler using the alignment laser.

After that alignment laser was blocked and the pumping at 910 nm was started. We observed a conical refraction ring along the propagation direction with a little adjustment of the Nd:KGW crystal. Figure 4.6 illustrates how the ring pattern changed along the propagation direction after the output coupler. Negative number indicates the image location inside the cavity and positive numbers indicates the image location outside the cavity. The ring shape is not clear because the ρ_0 is 1.53 and this is in excellent agreement with the experimentally obtained figure 4.2 (ρ_0 is 1.7) for the He-Ne laser.

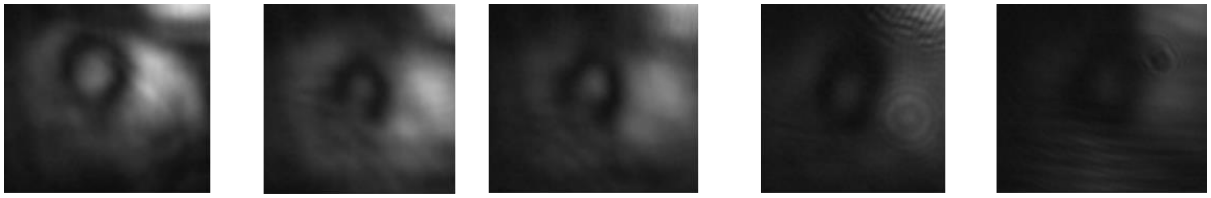

Figure 4.6: Change of the ring pattern along the propagation direction. Numbers indicate the distance of image plane with respect to the OC.

Our experimental results (a central spot inside the ring) are also supported by the figure 4.7 which represents the simulated ring intensity structure in the focal image plane for an unpolarized Gaussian incident beam with different ρ_0 values. If the ρ_0 is 0.5 then there is no ring and It is a simple Gaussian beam. For $\rho_0 = 2$, there is the ring with a central spot and it becomes a double ring with a very low intensity at the center when ρ_0 increases to 4. It should be noted that the intensity at the center is not zero for each of the presented conditions. As can be seen, our experimental results have a good agreement with the numerically simulated results. On the other hand, the central spot within the CR ring is also in good agreement with the previously reported simulation result of a CR laser cavity [40].

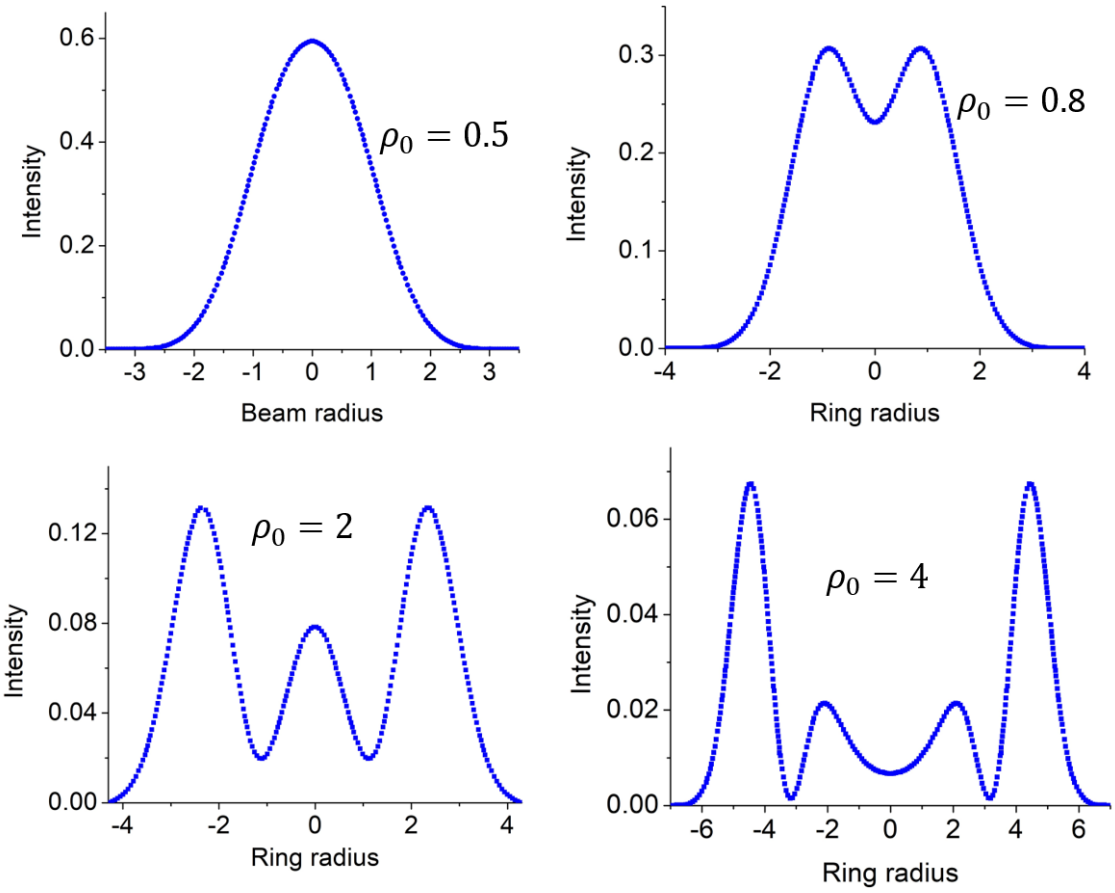

Figure 4.7: M.V. Berry et al. simulated ring structure in the focal image plane for an incident unpolarized Gaussian beam with different values of ρ_0 [7].

We have also observed the output beam after the OC with misaligned Nd:KGW crystal and without it in the cavity. In these cases we did not see any beam shapes similar to the CR pattern. This is shown in figure 4.8.

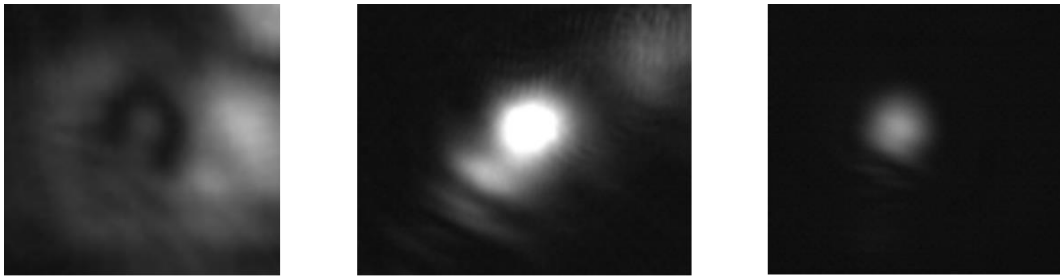

Figure 4.8: The output beam from the Nd:YVO laser with aligned, misaligned and without the Nd:KGW crystal.

The maximum absorbed pump power by the Nd:YVO crystal was 10.8 W for the incident pump power of 31.2 W. The laser produced the maximum laser output powers of 3.68 W, 3.68 W and 3.81 W for the case of the aligned Nd:KGW crystal along its optical axis (CR regime), misaligned crystal or without it inside the cavity, respectively. Insertion of the Nd:KGW crystal inside the cavity reduced the maximum output power due to additional intracavity losses. Slope efficiencies from linear fits were 42.26%, 42.75% and 44.13% and optical to optical efficiencies 34.07%, 34.07% and 35.28%, respectively. Figure 4.9 illustrates the output power vs the absorbed pump power for these three different conditions. Figure 4.10 shows the laser spectrum at 1064 nm.

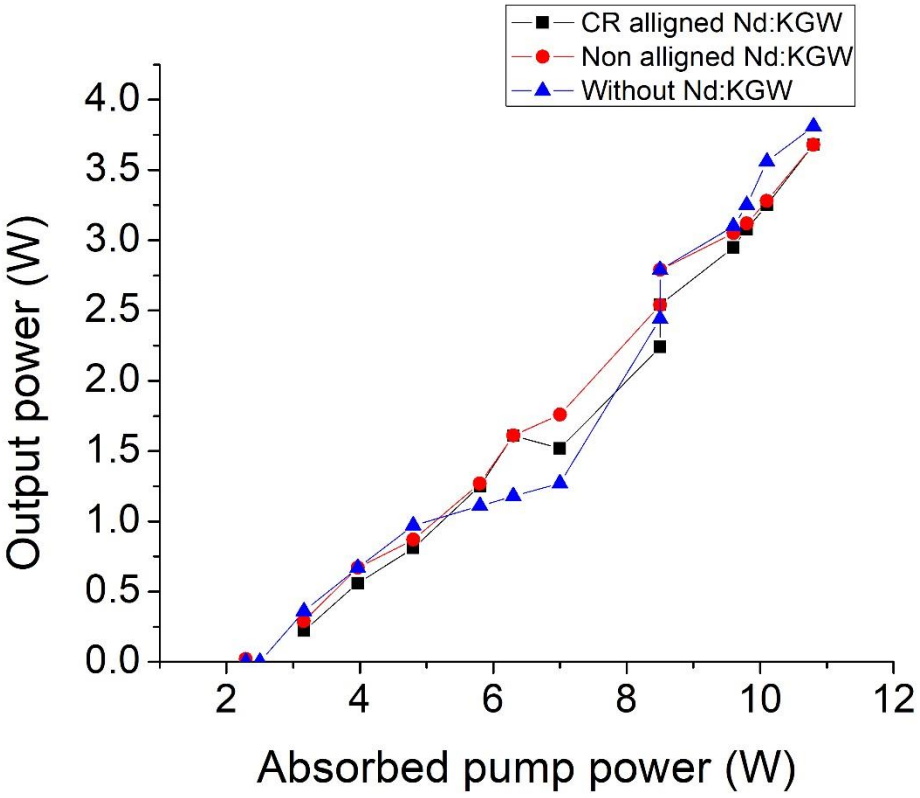

Figure 4.9: Output power vs the absorbed pump power for three different conditions.

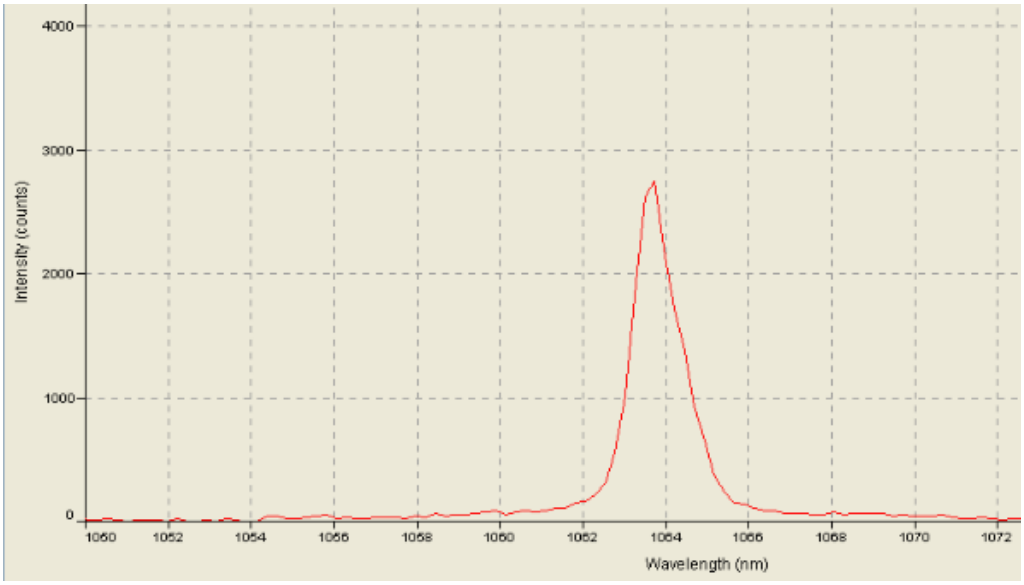

Figure 4.10: Laser spectrum at 1064 nm of the Nd:YVO/Nd:KGW laser.

Comparing with other reported non-CR continuous wave (CW) results shown in table 4.2 [43][9] it is obvious that the slope efficiency as well as optical to optical efficiency in our case are lower. This probably can be explained by the non-optimal value of the OC used in our

experiments. This points out to the fact that by increasing the transmission of the OC it should be possible to increase the power in the CR regime as well as improve slope efficiency and optical to optical efficiency. In addition, intracavity losses can be reduced by using a more compact cavity with lower number of mirrors.

Table 4.2: Comparison of reported results for the CW Nd:YVO4 lasers.

Author	Cavity mirror	Pump λ (nm)	O/P (W)	Slope efficiency (%)	Optical to optical efficiency (%)	OC (%)	Year
T. Waritanant et al.	3	914	3.52	66.9	56.8	10	2016
D. Sangla, et al.	3	914	11.5	80.7	78.7	15	2009
This work	4	910	3.81	44.1	35.3	5	2017

Finally, comparing with other reported CR lasers listed in Table 4.3, we have the highest laser output power as well as high slope efficiency. It is worth noting that the experimental conditions were not the same for all cases. Table 4.3 illustrates the input and output parameters of the reported CR lasers.

Table 4.3: Previously reported CR lasers.

Author	Pump λ (nm)	Cavity mirror	Gain medium	Power (W)	Slope efficiency (%)	Optical efficiency (%)	Ring radius R_o (μm)	$\rho_0 = \frac{R_0}{\omega_0}$
A. Abdolvand et al. (2010)	808	2	Nd:KGW	3.3	74	66	289	1.23/ 0.72
Y.V. Loiko et al. (2014)	805	2	Nd:KGW	-----	-----	30	204	2.06
R. Cattor et al. (2014)	1960	2	Ho:KYW	1.6	52	------	240	2.4
K.G. Wilcox et al. (2010)	808	2	Nd:KGW	0.53	30	24	246	1.23
A. Brenier (2016)	810	2	Nd:KGW	0.015	-----	------	52	1
This work (2017)	910	3	Nd:KGW	1.15	32	25.6	306	1.11
		4	Nd:KGW & Nd:YVO	3.68	44	34	306	1.5

Chapter 5: Conclusion and future works

5.1 Conclusion

In summary, we have successfully demonstrated the active and passive CR lasers with in-band pumping and observed conical refraction pattern for the output radiation. An active CR Nd:KGW laser operated at 1069 nm and in the non-CR regime lasing took place at 1067 nm with the output powers of 1.8 W and 1.15 W, respectively. The corresponding slope efficiencies were 46% and 32% and the optical to optical efficiencies were 40.1% and 25.6%, respectively. We have not observed the CR ring pattern in the output beam because of a large cavity mode size diameter inside of the crystal. From a passive CR laser setup (Nd:YVO + Nd:KGW) we obtained 3.68 W of output power with a CR ring pattern in the output beam. The slope efficiency was 42%. It was found that placing of a Nd:KGW crystal inside the cavity of a Nd:YVO laser did not have significant influence on laser power as well as efficiency. Therefore, such approach is an attractive pathway for power scaling of the CR lasers.

5.2 Future works

Further experiments can include optimization of the pump spot size to produce a clear CR pattern from the active CR laser as well as operating in high power regime and possibly nonlinear frequency conversion [44-48] or pulsed operation [49-52]. Also, conical refraction medium can be placed inside of a tunable laser cavity (such as Ti:sapphire) to get a wavelength tunable CR laser output.

References

[1] A. Brenier, “Lasing with conical diffraction feature in the KGd(WO4)2:Nd biaxial crystal,” Appl. Phys. B, vol. 122, no. 9, pp. 237, 2016.

[2] A. Turpin, Y. V. Loiko, T. K. Kalkandkiev, H. Tomizawa, and J. Mompart, “Super-Gaussian conical refraction beam,” Opt. Lett., vol. 39, no. 15, pp. 4349–4352, 2014.

[3] G. S. Sokolovskii, V. Y. Mylnikov, S. N. Losev, K. A. Fedorova, and E. U. Rafailov, “Conical refraction of a high-M2 laser beam,” Proc. of SPIE, vol. 10090, pp. 100901R-1, 2017.

[4] A. A. Demidovich, A. P. Shkadarevich, M. B. Danailov, P. Apai, T. Gasmi, V. P. Gribkovskii, A. N. Kuzmin, G. I. Ryabtsev, and L. E. Batay, “Comparison of cw laser performance of Nd : KGW, Nd : YAG, Nd : BEL, and Nd : YVO4 under laser diode pumping,” Appl. Phys. B, vol. 67, no. 1, pp. 11–15, 1998.

[5] Y. Kalisky, L. Kravchik, and C. Labbe, “Repetitive modulation and passively Q-switching of diode-pumped Nd-KGW laser,” Opt. Commun., vol. 189, no. 1, pp. 113–125, 2001.

[6] M. V. Berry, M. R. Jeffrey, and J. G. Lunney, “Conical diffraction: observations and theory,” Proc. R. Soc. A Math. Phys. Eng. Sci., vol. 462, no. 2070, pp. 1629–1642, 2006.

[7] M. V. Berry and M. R. Jeffrey, “Conical diffraction: Hamilton’s diabolical point at the heart of crystal optics,” Prog. Opt., vol. 50, pp. 13–50, 2007.

[8] O. Müller, “This is the story of conical refraction that was discovered more than 150 years ago and only now will come to real first applications,” Vis. Cryst. Technol. AG, pp. 1–6.

[09] T. Waritanant and A. Major, “Thermal lensing in Nd:YVO4 laser with in-band pumping at 914 nm,” Appl. Phys. B, vol. 122, no. 5, pp. 135, 2016.

[10] R. C. Talukder, M. Z. E. Halim, T. Waritanant, and A. Major, “Multi-watt continuous wave Nd : KGW laser with hot band diode pumping,” Opt. Lett., vol. 41, no. 16, pp. 3810-3812, 2016.

[11] T. K. Kalkandjiev and M. A. Bursukova, “Conical refraction: an experimental introduction,” Phot. Manag. III, vol. 6994, pp. 69940B, 2008.

[12] T. Waritanant and A. Major, “High efficiency passively mode-locked Nd:YVO4 laser with direct in-band pumping at 914 nm,” Opt. Express, vol. 24, no. 12, pp. 12851-12855, 2016.

[13] J. Hellstrom, H. Henricsson, V. Pasiskevicius, U. Bunting, and D. Haussmann, "Polarization-tunable Yb : KGW laser based on internal conical refraction," Opt. Lett., vol. 32, no. 19, pp. 2783–2785, 2007.

[14] S. D. Grant, S. A. Zolotovskaya, W. A. Gillespie, T. K. Kalkandjiev, and A. Abdolvand, "Azimuthally and radially polarized light in conical diffraction," Opt. Lett., vol. 39, no. 7, pp. 1988–1991, 2014.

[15] C. V. Raman, V. S. Rajagopalan and T. M. K. Nedungadi, "Conical refraction in naphthalene crystals," Proc. Indian Acad. Sci.-Sec. A, vol. 14, no. 3, pp. 221-227, 1941.

[16] J. G. Lunney and D. Weaire, "The ins and outs of conical refraction," Europhys. News, vol. 37, no. 3, pp. 26–29, 2006.

[17] A. T. Avil, "Conical refraction : fundamentals and applications," PhD Thesis, Universitat Aut`onoma de Barcelona, 2015.

[18] A. Abdolvand, K. G. Wilcox, T. K. Kalkandjiev, and E. U. Rafailov, "Conical refraction Nd:KGd(WO4)2 laser," Opt. Express, vol. 18, no. 3, pp. 2753-2759, 2010.

[19] T. David, "On the conical refraction of hydromagnetic waves in plasma with anisotropic thermal pressure," Physics of Plasmas, vol. 3, no. 3, pp. 800-803, 1996.

[20] Ablowitz, J. Mark, D. Sean, Nixon, and Yi Zhu, "Conical diffraction in honeycomb lattices," Physical Review A, vol. 79, no. 5, pp. 053830, 2009.

[21] Leykam, Daniel, Omri Bahat-Treidel, and A. S. Desyatnikov, "Pseudospin and nonlinear conical diffraction in Lieb lattices," Physical Review A, vol. 86, no. 3, pp. 031805, 2012.

[22] M. C. Pujol, R. Solé, J. Massons, Jna Gavaldà, X. Solans, C. Zaldo, F. Díaz, and M. Aguiló, "Structural study of monoclinic KGd(WO4)2 and effects of lanthanide substitution," Journal of Appl. Crystallogr., vol. 34, no. 1, pp. 1–6, 2001.

[23] I. V. Mochalov, "Laser and nonlinear properties of the potassium gadolinium tungstate laser crystal KGd(WO4)2:Nd3+-(KGW:Nd)," Opt. Eng., vol. 36, no. 6, pp. 1660-1670, 1997.

[24] P. Loiko, S. J. Yoon, J. M. Serres, X. Mateos, S. J. Beecher, R. B. Birch, V. G. Savitski, A. J. Kemp, K. Yumashev, U. Griebner, and V. Petrov, "Temperature-dependent spectroscopy and microchip laser operation of Nd:KGd(WO4)2," Optical Materials, vol. 58, pp. 365–372, 2016.

[25] J. D. R. Moncorge, B. Chambon, J. Y. Rivoire, N. Garnier, E. Descroix, P. Laporte, H. Guillet, S. Roy, J. Mareschal, and D. Pelenc, "Nd doped crystals for medical laser application," Optical Materials, Vol. 8, no. 1-2, pp. 109–119, 1997.

[26] A. Y. Ibrahim, "Studies of diode-pumped solid-state lasers based on Nd:KGW and

Nd:YAG, ” MSc thesis, University of Khartoum, 1996.

[27] C. F. Phelan, D. P. O’Dwyer, Y. P. Rakovich, J. F. Donegan, and J. G. Lunney, “Conical diffraction and Bessel beam formation with a high optical quality biaxial crystal,” Opt. Express, vol. 17, no. 15, pp. 12891-12899, 2009.

[28] R. C. Talukder, “High power continuous wave Nd:KGW laser with low quantum defect diode pumping,” MSc thesis, University of Manitoba, 2016.

[29] A. S. Grabtchikov, A. N. Kuzmin, V. A. Lisinetskii, V. A. Orlovich, G. I. Ryabtsev, and A. A. Demidovich, “All solid-state diode-pumped Raman laser with self-frequency conversion,” Appl. Phys. Lett., vol. 75, no. 24, pp. 3742-3744, 1999.

[30] A. Major, D. Sandkuijl, and V. Barzda, “Efficient frequency doubling of a femtosecond Yb:KGW laser in a BiB_3O_6 crystal,” Opt. Express, vol. 17, no. 14, pp. 12039-12042, 2009.

[31] A. Major, J. S. Aitchison, P. W. E. Smith, F. Druon, P. Georges, B. Viana, and G. P. Aka, “Z-scan measurements of the nonlinear refractive indices of novel Yb-doped laser crystal hosts,” Appl. Phys. B, vol. 80, no. 2, pp. 199-201, 2005.

[32] A. Major, D. Sandkuijl, and V. Barzda, “A diode-pumped continuous-wave Yb:KGW laser with Ng-axis polarized output,” Laser Phys. Lett., vol. 6, no. 11, pp. 779, 2009.

[33] A. S. Kumaran, “Growth of pure and rare earth (Nd^{3+} and Yb^{3+}) doped double tungstates KGd(WO4)2 and KY(WO4)2 and their characterization,” PhD thesis, Anna University Chennai, 2008 (http://hdl.handle.net/10603/43149).

[34] H. J. Zhang, L. Zhu, X. L. Meng, Z. H. Yang, C. Q. Wang, W. T. Yu, Y. T. Chow, and M. K. Lu, “Thermal and laser properties of Nd : YVO4 crystal,” Crystal Research and Technology, vol. 34, no. 8, pp. 1011–1016, 1999.

[35] X. Peng, A. Asundi, Y. Chen, and Z. Xiong, “Study of the mechanical properties of Nd:YVO4 crystal by use of laser interferometry and finite-element analysis,” Appl. Opt., vol. 40, no. 9, pp. 1396–1403, 2001.

[36] T. Waritanant, “Highly efficient diode-pumped lasers based on in-band pumping of Nd : YVO4 crystal,” PhD thesis, University of Manitoba, 2017.

[37] K. G. Wilcox, A. Abdolvand, T. K. Kalkandjiev, and E. U. Rafailov, “Laser with simultaneous Gaussian and conical refraction outputs,” Appl. Phys. B, vol. 99, no. 4, pp. 619–622, 2010.

[38] R. Cattoor, I. Manek-Honninger, D. Rytz, L. Canioni, and M. Eichhorn, “Laser action along and near the optic axis of a holmium-doped KY(WO4)2 crystal,” Opt. Lett., vol. 39, no. 22, pp. 6407–6410, 2014.

[39] G. S. Sokolovskii, D. J. Carnegie, T. K. Kalkandjiev, and E. U. Rafailov, "Conical refraction: new observations and a dual cone model," Opt. Express, vol. 21, no. 9, pp. 11125-11131, 2013.

[40] Y. V. Loiko, G. S. Sokolovskii, D. Carnegie, A. Turpin, J. Mompart, and E. U. Rafailov, "Laser beams with conical refraction patterns," Proc. SPIE, vol. 8960, pp. 89601Q, 2014.

[41] C. F. Phelan, K. E. Ballantine, P. R. Eastham, J. F. Donegan, and J. G. Lunney, "Conical diffraction of a Gaussian beam with a two crystal cascade," Opt. Express, vol. 20, no. 12, pp. 13201-13207, 2012.

[42] H. Mirzaeian, S. Manjooran, and A. Major, "A simple technique for accurate characterization of thermal lens in solid state lasers," Proc. SPIE, vol. 9288, pp. 928802, 2014.

[43] D. Sangla, M. Castaing, F. Balembois, and P. Georges, "Highly efficient Nd:YVO4 laser by direct in-band diode pumping at 914 nm," Opt. Lett., vol. 34, no. 14, pp. 2159-2161, 2009.

[44] H. Zhao, I. T. Lima, and A. Major, "Near-infrared properties of periodically poled $KTiOPO_4$ and stoichiometric MgO-doped $LiTaO_3$ crystals for high power optical parametric oscillation with femtosecond pulses," Laser Phys., vol. 20, no. 6, pp. 1404-1409, 2010.

[45] I. T. Lima, V. Kultavewuti, and A. Major, "Phasematching properties of congruent MgO-doped and undoped periodically poled $LiNbO_3$ for optical parametric oscillation with ultrafast excitation at 1 μm," Laser Phys., vol. 20, no. 1, pp. 270-275, 2010.

[46] R. Akbari and A. Major, "Optical, spectral and phase-matching properties of BIBO, BBO and LBO crystals for optical parametric oscillation in the visible and near-infrared wavelength ranges," Laser Phys., vol. 23, no. 3, pp. 035401, 2013.

[47] S. Manjooran, H. Zhao, I. T. Lima, and A. Major, "Phase-matching properties of PPKTP, MgO:PPSLT and MgO:PPcLN for ultrafast optical parametric oscillation in the visible and near-infrared ranges with green pump," Laser Phys. vol. 22, no. 8, pp.1325–1330, 2012.

[48] H. Zhao, K. Sukhoy, I. T. Lima, and A. Major, "Generation of green second harmonic with 60% conversion efficiency from a Q-switched microchip laser in MgO:PPLN crystal," Laser Phys., vol. 9, no. 5, pp. 355, 2012.

[49] M. Z. E. Halim, R. C. Talukder, T. Waritanant, and A. Major, “Passive mode-locking of a Nd:KGW laser with hot band diode pumping,” Laser Physics Letters, vol. 13, no. 10, pp. 105003, 2016.

[50] S. Ghanbari, R. Akbari, and A. Major, “Femtosecond Kerr-lens mode-locked Alexandrite laser,” Optics Express, vol. 24, no. 13, pp. 14836-14840, 2016.

[51] A. Major, L. Giniūnas, N. Langford, A. I. Ferguson, D. Burns, E. Bente, and R. Danielius, “Saturable Bragg reflector-based continuous-wave mode locking of Yb:KGd(WO4)2 laser,” J. Mod. Opt., vol. 49, no. 5-6, pp. 787–793, 2002.

[52] R. Akbari, K. A. Fedorova, E. U. Rafailov, and A. Major, “Diode-pumped ultrafast Yb:KGW laser with 56 fs pulses and multi-100 kW peak power based on SESAM and Kerr-lens mode locking,” Appl. Phys. B, vol. 123, no. 4, pp. 123, 2017.